Prediction of Multicomponent Gas Adsorption Equilibrium Using Ideal Adsorbed Solution Theory for Direct Air Capture

by

Trevor Ciha

A Thesis Presented in Partial Fulfillment
of the Requirements for the Degree
Master of Science

Approved April 2022 by the
Graduate Supervisory Committee:

Shuguang Deng, Chair
Michael Machas
Huei-Ping Huang

ARIZONA STATE UNIVERSITY

May 2022

ABSTRACT

Adsorption equilibrium is an important metric used to assess adsorbent performance for gas mixture separation processes. Gas adsorption processes such as carbon capture are becoming more urgent as climate change and global warming accelerate. To speed up and reduce the cost of research on adsorbent materials and adsorption processes, I developed an open-source Python code that generates mixed gas adsorption equilibrium data using pure gas adsorption isotherms based on the ideal adsorbed solution theory (IAST). The major efforts of this M.S. research were placed on adding additional components to the mixture models since most other publications focused on binary gas mixtures. Generated mixed-gas equilibrium data were compared to experimentally collected data in order to validate the multicomponent IAST model and to determine the accuracy of the computer codes developed in this work. Additional mixed-gas equilibrium data were then generated and analyzed for trends in the data for humid flue gas conditions, natural gas processing conditions, and hydrogen gas purification conditions. For humid flue gas conditions, neither the analyzed Mg-MOF-74 nor the Zeolite 13X were shown to be suitable for use. For natural gas processing conditions, the Zeolite 13X was determined to be a much better candidate for use than the MIL-101. For hydrogen gas purification conditions, the Zeolite 5A was determined to be a better adsorbent for use than CD-AC due to the Zeolite 5A's much lower adsorption of H_2.

ACKNOWLEDGMENTS

First, thank you to Dr. Shuguang Deng, the chair of my M.S. thesis committee. Dr. Deng has provided a ton of advice and help over the course of the last two years, and I am extremely grateful for all of that, along with your patience while working with me. Next, I'd like to thank Dr. Michael Machas and Dr. Huei-Ping Huang, my other two committee members, who both generously agreed to help with proofreading my thesis and taking part in my thesis defense. Thank you as well to Dr. Mai Xu, who provided a lot of assistance with various lab-related things, provided his collected data for analysis, and was generally extremely helpful whenever I talked with him.

Thanks to all of my family for being extremely supportive in everything that I do, and specifically my parents, Jason and Lori, for always being there for me. Even though we moved around a lot, you were always my rock and made sure that I would thrive in whatever new place we went to. You did an incredible job of supporting me without being overbearing and helped shape me into the man I am today, and for that, I cannot thank you enough.

Thanks to all of my friends, who have been with me through my highs and lows, and helped me navigate the last several years of my life. It's insane to me just how close people can get within a year or two, as has happened in college. I'd like to give a shoutout to my chemical engineering friends: Xavier, Dylan, Adam, and Sean. You guys made this possible and I honestly don't know that I would have made it through this degree program without all of you. To Xavier in particular, I appreciate you so much more than I can express. We've done everything together for the last 3 years and we've both been there through all of our highs and all of our lows, and it's been far more

bearable and enjoyable with you at my side. To all my closest friends, including those I don't have the space to individually thank, I appreciate everything we've been through together more than words can express. I hope you know that I will always be here for you if you need me, just like you've all been there for me when I needed it.

TABLE OF CONTENTS

Page

LIST OF FIGURES

Figure Page

Figure Page

Figure Page

CHAPTER 1

INTRODUCTION

Climate change has been discussed as an issue of great importance for decades now, without an adequate investment of research funding or time being devoted to helping mitigate its effects. The most direct cause of rapidly increasing climate change is the accumulation of large amounts of greenhouse gases in the Earth's atmosphere. Of those greenhouse gases, up to 76% of them are estimated to be carbon dioxide alone (US EPA, 2016). The largest contributor of carbon dioxide to the atmosphere is the energy sector, which is the result of burning fossil fuels such as oil, gasoline, and natural gas to provide energy (Choi et al., 2009).

One potentially promising stopgap for the issue of climate change is carbon capture and storage via methods such as direct air capture. Carbon capture and storage are more of a stopgap solution than an actual solution because it requires the storage of large amounts of gases such as carbon dioxide, which takes up both space and energy, especially since the most space efficient means of storage, storing it as a liquid, requires the most energy to accomplish (*Carbon Storage FAQs*, n.d.). The process of carbon capture and storage via direct air capture has three general steps to it, those being gas capture, transportation, and storage. This study will focus solely on the capture step, since removing carbon dioxide from the atmosphere is more pressing than efficiently storing it. Additionally, the capturing step has been the one most scrutinized and is typically seen as the limiting factor in carbon capture and storage.

The problems faced by scientists working to develop more advanced carbon capture techniques are similar to those faced by scientists in most research endeavors: a

lack of time and money, as mentioned earlier. This study seeks to both advance the knowledge of carbon capture technologies while also decreasing the time and funding required to make further research advancements by developing code that will perform quick analysis on potential adsorbents, allowing for scientists to put more focus on the sorbents showing the most promise. The developed code is meant to serve as a piece of the bigger picture in adsorbent research by being open source and performing its intended functionality quickly and easily.

CHAPTER 2

ADSORPTION BACKGROUND

Gas separation processes have always been some of the more complex "simple" separation processes due to gases being comparatively more difficult to work with than liquids or solids. However, there are still several methods of gas separation, some of which are cryogenic distillation, membrane separation, and adsorption. The focus of this study is on adsorption processes, as most other gas separation processes, including cryogenic distillation and membrane separation, are held back by issues such as extreme energy intensity or slow separation rates (Carta, 2015).

Adsorption is a process in which multiple components of a fluid mixture, in this case, a gaseous mixture, flow into an apparatus packed with the sorbent and adhere to the surface of, or are adsorbed onto the sorbent. The components being adsorbed are also referred to as sorbates (Geankoplis, 2018). Since the goal of adsorption is to separate gases from one another, a "good" sorbent is one that selectively adsorbs only the desired components, therefore allowing for the rest of the gas stream to exit the apparatus far purer than it entered. There are two general types of adsorption processes, those being chemisorption and physisorption. In physisorption, adsorption is governed by van der Waals forces and is generally weaker and easily reversible. In contrast, chemisorption is more akin to the formation of chemical bonds, is much stronger, and is far harder to reverse than physisorption (Ben-Mansour et al., 2016). Due to the convenient reversibility of physisorption, it is generally more widely used for carbon capture purposes since the sorbent can be reused many times over a long time period.

Adsorbents

Adsorption offers many parameters and methods that allow it to be fine-tuned for a specific application. Of these parameters, none has as large of an impact as the actual sorbent used. The three most common types of sorbents used are zeolites, metalorganic frameworks (MOFs), and activated carbons. All three types of sorbents come with pros and cons, and as such, all must be accounted for in this study. Zeolites are crystalline aluminosilicates of alkali or alkali earth elements, typically sodium, potassium, or calcium. The main structural units of zeolites are SiO_4 and AlO_4, which are arranged into crystalline frameworks (Yang, 2003). An example of a structural unit cell of a type X zeolite can be seen below in Figure 1.

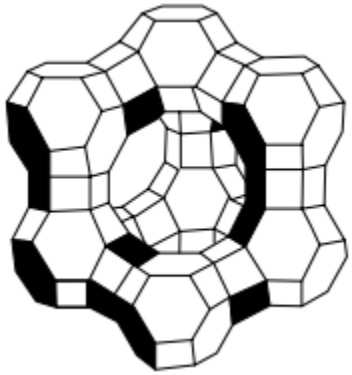

Figure 1: Zeolite Type X Unit Cell (Yang, 2003)

MOFs are a relatively new class of porous materials that was first developed in the late 1980s. MOFs are porous crystalline materials constructed from metal-containing nodes that are linked through organic ligands (Ben-Mansour et al., 2016). The unique blend of organic and inorganic materials present in MOFs makes them very flexible. An example of a MOF is shown below in Figure 2.

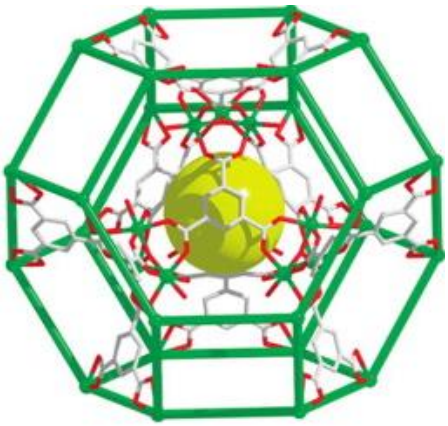

Figure 2: Structure of CPM-5 Type MOF (Sabouni et al., 2013)

Activated carbon sorbents are a sorbent category that typically is characterized by their extremely high micropore and mesopore volumes, which are the most important pore sizes for gas separation due to the small size of gas molecules relative to molecules in other states. Activated carbon sorbents can vary greatly depending on the synthesis procedures and what the precursor material was, as they can be prepared from a huge variety of biomaterials such as wood, peat, or algae (Marsh & Rodríguez-Reinoso, 2006). An example of activated carbon is shown below in Figure 3.

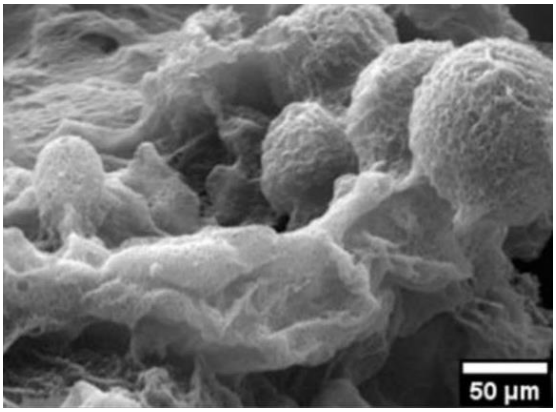

Figure 3: SEM Image of Activated Carbon from Palm Date Seeds (Alazmi et al., 2021)

Adsorption Isotherms

One of the most widely used metrics used in adsorbent selection is adsorption isotherm modeling. An adsorption isotherm is a method of describing a sorbent's adsorptive capacity and equilibrium behavior across a range of pressures at a constant temperature. An example of an adsorption isotherm is shown below in Figure 4 (Wang & LeVan, 2010).

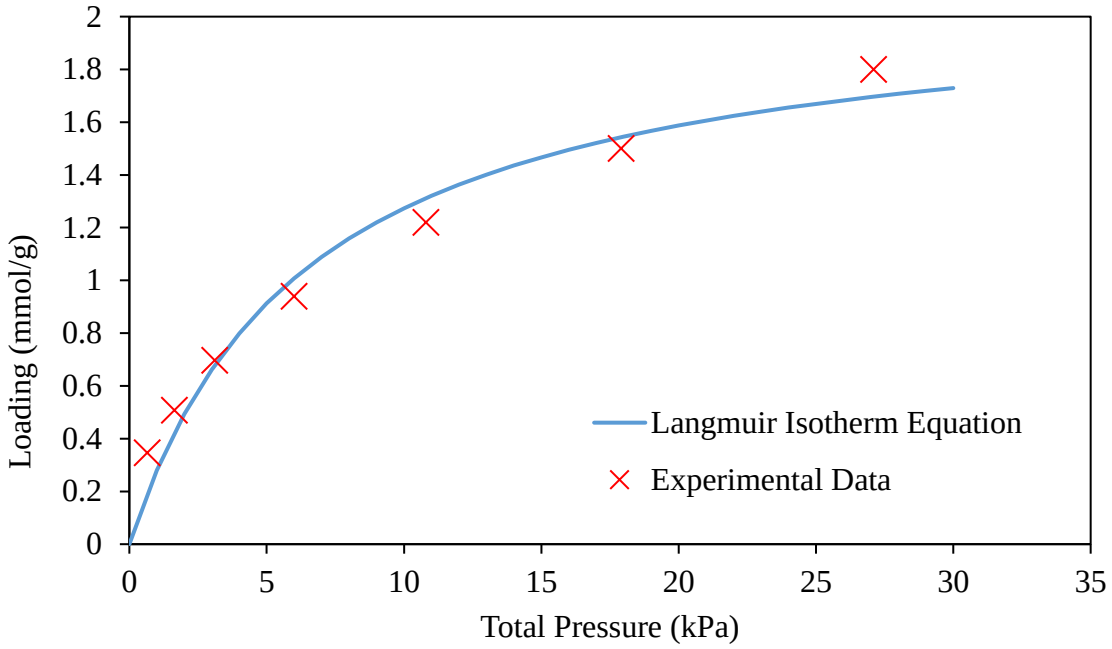

Figure 4: Example Experimental Data and Fitted Langmuir Isotherm Equation

A feature of adsorption isotherms is that their data can be fitted to an adsorption isotherm equation and expressed as a function of pressure. Using this equation, the adsorptive capacity for a sorbent at a specific temperature can then be predicted at any pressures, including those not actually tested during experimentation. Isotherm equations can be used to both interpolate and extrapolate from the experimental data, although they are typically better at interpolation. There have been many isotherm equations created,

although one of the most widely used continues to be one of the first ones, that being the Langmuir isotherm equation. The Langmuir isotherm equation continues to see widespread usage due to its simplicity and general accuracy. The Langmuir isotherm equation is shown below in Equation 1 for a pure component adsorption isotherm.

$$C_{\mu} = C_{\mu s} \frac{bP_i}{1+bP_i} \quad (1)$$

An extremely simplistic way of predicting mixed-gas adsorption performance is by adding together the individual adsorptive capacities of the gaseous components, though this presents large errors and is generally not used for anything more in-depth than a brief overview.

Pure gas isotherms are the only isotherms that can be relatively easily generated experimentally. Mixed-gas isotherms, which can be experimentally tested, require much more complex methodologies than pure gas isotherms. Some examples of these techniques are the zero-length column technique, the frequency response technique, and the isotope exchange technique (Ray, 1996). However, all of these methods are measuring the equilibrium Gibbsian surface excesses instead of the actual amounts adsorbed, though those can then be calculated using the Gibbsian surface excesses (Sircar, 1999). One major downside to these methods is there is inherently no control over the final equilibrium state in the experiment, which results in data that can be somewhat random in comparison to pure gas equilibrium data (Sircar, 2006). Due to these difficulties, along with the high interest in adsorption isotherms, multiple theories have been developed to model multi-component adsorption isotherms based on pure adsorption isotherm data. These theories have a variety of ways of accounting for interactions between adsorbate molecules of different components. The specific theory

utilized for this thesis is the Ideal Adsorbed Solution Theory (IAST), which will be discussed thoroughly in Chapter 3. Alternatives to IAST include the vacancy solution theory and the Polanyi adsorption potential theory, among many others (Dubinin, 1960; Nieszporek, 2006).

Since the Earth's atmosphere is comprised primarily of N_2, researchers focused on direct air carbon capture are typically interested in binary mixtures of N_2 and CO_2. This results in a heavy emphasis being placed on binary mixture adsorption isotherms, with little emphasis on any number of components higher than two. However, this study focuses on ternary mixtures and mixtures of more than two components mainly because a third component can significantly impact the adsorptive performance of other components. Specifically, many adsorbents perform very differently when humidity levels rise and H_2O concentrations increase. For adsorption to be viable regardless of location, it is important to understand how different humidity levels affect adsorptive performance since humidity levels are dramatically different in different regions of the planet.

CHAPTER 3

MATHEMATICAL MODELING & THEORY

It is important that any model applied for the prediction of multicomponent adsorption equilibrium data is thermodynamically consistent (Myers & Prausnitz, 1965). Thus, in deriving the desired model, in this case, the Ideal Adsorbed Solution Theory (IAST), the starting point will be the differential form of the fundamental Gibbs free energy, G, of the adsorbed phase such that

$$dG = -SdT + Ad\pi + \sum \mu_i dn_i \tag{2}$$

Thus, the intensive variables for the Gibbs free energy are spreading pressure, π, temperature, T, and molar composition, n_i. At a constant spreading pressure and temperature, the equation can be simplified and integrated to be

$$G = \sum n_i \mu_i \tag{3}$$

Using the two-dimensional gas model (Thiele, 1953), the ideal gas law is obeyed at low surface coverages and the following expression for the spreading pressure is obtained

$$\pi A = n_T RT \tag{4}$$

where A is the area of the sorbent, R is the ideal gas constant, and n_T is the total adsorbed moles. As mentioned previously, the intensive variables, in this case, are π, T, and n_i. This then allows an expression for the molar Gibbs free energy change upon mixing, g^m, at constant T and π, which is given by

$$g^m(T, \pi, x_1, \dots) = RT \sum x_i \ln \gamma_i x_i \tag{5}$$

The change due to mixing for an extensive molar property, in this case, molar Gibbs free energy, can also be expressed as the difference between the total molar Gibbs free energy

of the mixture and the sum of the individual components' molar Gibbs free energy prior to mixing, such that

$$g^m(T, \pi, x_1, \dots) = g(T, \pi, x_1, \dots) - \sum x_i g_i^0(T, \pi) \quad (6)$$

where $g_i^0(T, \pi)$ is the molar Gibbs free energy for pure i at T and π. Equations 3, 5, and 6 can then be combined and rearranged to obtain an expression for the chemical potential of an individual component, μ_i, and

$$\mu_i(T, \pi, x_1, \dots) = g_i^0(T, \pi) + RT \ln \gamma_i x_i \quad (7)$$

In Equation 7, $g_i^0(T, \pi)$ is the molar Gibbs free energy of component i, when i is adsorbed in the absence of other gases at temperature T and spreading pressure π. An expression for this quantity can be derived in relation to its value at a reference state, $g_i^0(T)$ and

$$g_i^0(T, \pi) = g_i^0(T) + RT \ln P_i^0 \quad (8)$$

Substituting Equation 8 into Equation 7 then yields

$$\mu_i(T, \pi, x_1, \dots) = g_i^0(T) + RT \ln P_i^0(\pi) * RT \ln \gamma_i x_i \quad (9)$$

which gives the chemical potential for the adsorbed phase of component i. A similar equation can be derived for the chemical potential of the gas phase in relation to the same reference state as before, as

$$\mu_i(T, P, y_i) = g_i^0(T) + RT \ln P y_i \quad (10)$$

When applying the criterion that the chemical potential for any component i in the adsorbed phase must be equal to its chemical potential in the gas phase, an equation of equilibrium can be written as

$$P y_i = P_i^0(\pi) \gamma_i x_i \quad (11)$$

The Gibbs adsorption isotherm (Hill, 1949) is

$$-Ad\pi + \sum n_i d\mu_i = 0 \tag{12}$$

For a pure component, substituting Equation 10 into Equation 12 and then integrating gives

$$\pi(P_i^0) = \frac{RT}{A}\int_0^{P_i^0} \frac{n_i^0}{P_i} dP_i \tag{13}$$

It is at this point that the assumptions central to IAST come into play. The three major assumptions used to develop IAST are (Walton & Sholl, 2015):

(1) Adsorbate molecules in the mixture have equal access to the entire surface

(2) The adsorbent is homogeneous

(3) The adsorbed phase is an ideal solution in which intermolecular interactions are equivalent in strength to one another

Two important mathematical simplifications result from these assumptions. The first is that by assuming an ideal solution, the activity coefficient for each component, γ_i, is equal to 1. This allows for Equation 11 to be simplified to

$$Py_i = P_i = P_i^0(\pi)x_i \tag{14}$$

The second important relationship comes from assuming adsorbate molecules have equal access to the entire surface and that the adsorbent is homogeneous. By making this assumption, the pure component spreading pressures, π_i, are equal and are equal to the total spreading pressure of the mixture, which can be written as (Simon et al., 2016)

$$\pi_i = \pi_{i+1} = \pi_{i+2} \ldots = \pi \tag{15}$$

By combining Equation 13 with Equation 15 and substituting the adsorbed concentration of component i, $C_{\mu i}$, in for n_i, an equation relating the adsorbed concentration of each component at the same spreading pressure can be written as

$$\frac{\pi A}{RT} = \int_0^{P_1^0} \frac{C_{\mu 1}}{P_1} dP_1 = \int_0^{P_2^0} \frac{C_{\mu 2}}{P_2} dP_2 = \cdots = \int_0^{P_i^0} \frac{C_{\mu i}}{P_i} dP_i \tag{16}$$

which, when combined with an isotherm equation such as the Langmuir isotherm equation shown in Equation 1, yields a system of equations that can be solved to determine the pure pressure of each component. The exact algorithm and solving process used in the code accompanying this thesis will be detailed in Chapter 4.

After determining the pure pressure of each component, the adsorbed concentration for that component can be determined using the same isotherm equation as was used to calculate the pure pressure and can be expressed as

$$C_{\mu i}^0 = C_{\mu s} \frac{bP_i^0}{1+bP_i^0} \tag{17}$$

where $C_{\mu i}^0$ is the hypothetical adsorbed concentration of the pure component in the mixture. Knowing the hypothetical adsorbed concentration of the individual components and their associated adsorbed phase mole fractions, x_i, the total amount adsorbed, $C_{\mu T}$, can be calculated as (Do, 1998)

$$\frac{1}{C_{\mu T}} = \sum_{i=1}^{n} \frac{x_i}{C_{\mu i}^0} \tag{18}$$

Once the total amount adsorbed has been calculated, then the actual adsorbed concentration of each individual component can be calculated using

$$C_{\mu i} = x_i C_{\mu T} \tag{19}$$

where $C_{\mu i}$ is the actual adsorbed concentration of component i.

CHAPTER 4

CODE ALGORITHM & STRUCTURE

The first step in writing code is selecting a language to write in. Given the ever-increasing number of coding languages available, this can sometimes be a time-consuming process. Since the goal of this project was to make the source code as readily available as possible, Python was the selected coding language. Python was selected because of its flexibility and applications in a wide variety of fields, making it easy to work with and easily accessible. Python is a relatively high-level language that allows for the importation of useful packages and functions created by others, making it an extremely powerful tool for people interested in writing code but not interested in building things from the ground up.

The algorithm used to create the Python files attached in Appendix A, Appendix B, and Appendix C is shown in a high-level diagram in Figure 5 below. Three distinct Python files were used to improve overall readability and organization. Additionally, they each perform slightly different functions. The file in Appendix A is used to retrieve the adsorption equilibrium data and simulation parameters, the file in Appendix B is used to fit an isotherm equation to the equilibrium data, and the file in Appendix C is used to perform the necessary IAST calculations. In Figure 5 below, the orange diamonds represent loops or logic controls, the blue rhombuses represent user input or output to the console, and the gray rectangles represent calculations performed by the code.

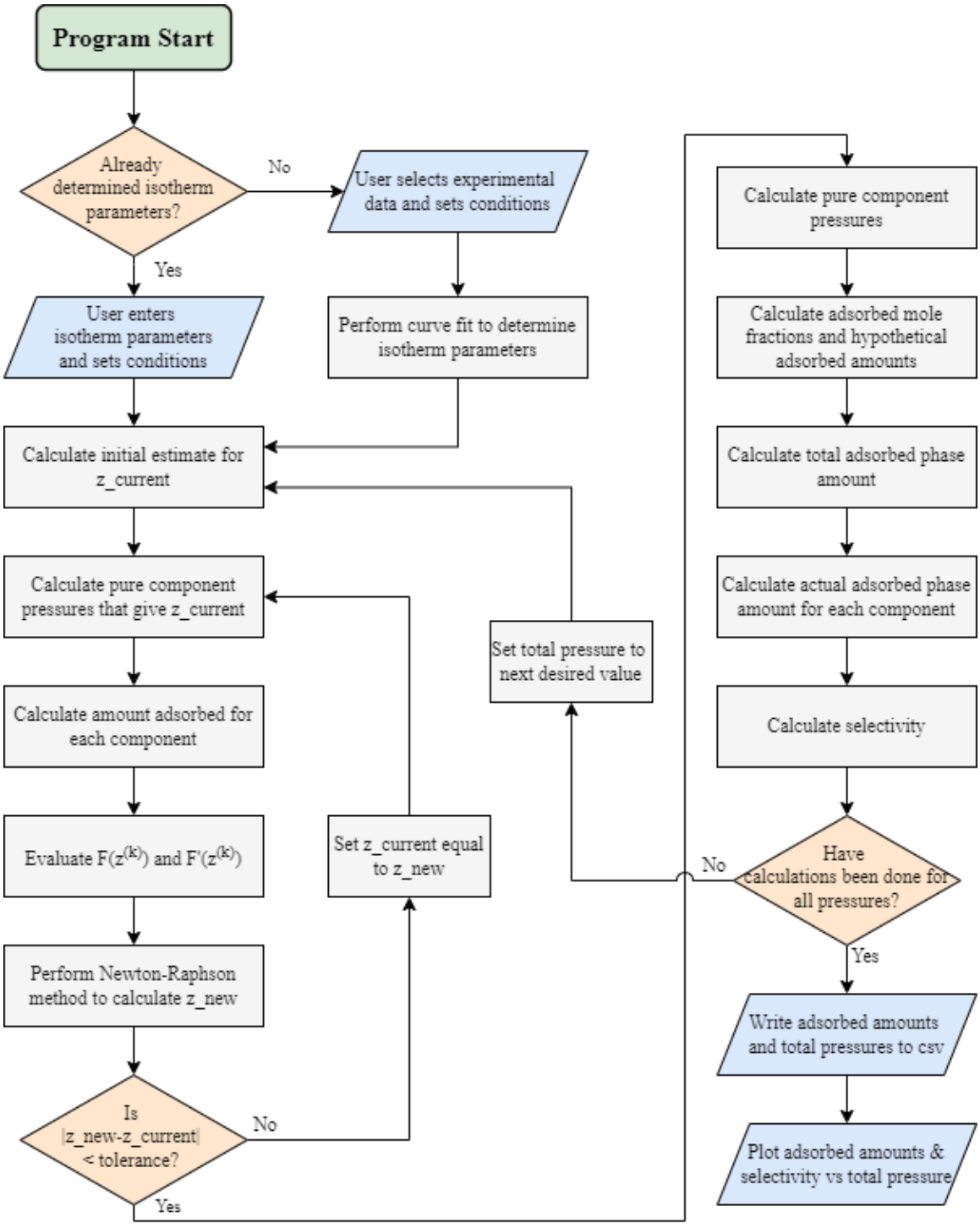

Figure 5: Flowchart Displaying Code Algorithm

The code was written to work with either pure component experimental equilibrium data or with isotherm parameters that were previously obtained by the user. Once the program is started, it prompts the user to check if the isotherm parameters have already been determined or not. If they have, the user then selects the isotherm equation type and inputs the parameters for the isotherm along with the conditions for the simulated multicomponent adsorption equilibrium data. The pressure minimum, maximum, and interval can all be set, as can the gaseous mole fraction for each component. If the isotherm parameters have not already been attained, the user will need to select the proper .csv files containing the pure component equilibrium data for each component. The user will additionally need to specify the same parameters for the generated multicomponent adsorption equilibrium data as were specified for the case where the isotherm parameters were already known. The code will then fit the experimental data from the .csv files for each component to the selected isotherm equation and store the determined parameters.

After all of the parameters have been determined, the code then begins to perform many calculations in a row without user input. To calculate the initial estimate for the spreading pressure, z_current, a modified version of Equation 13 can be used. Instead of using the pure component pressures, a molar average of all the adsorbed amounts at the total pressure can be taken. This equation can be written as

$$z = \frac{\pi A}{RT} = \sum_{i=1}^{N} y_i \int_0^P \frac{C_{\mu i}}{P_i} dP_i \tag{20}$$

where z is the reduced spreading pressure, which is the spreading pressure combined with the other constants (*A*, *R*, and *T*) to simplify calculations.

After the initial estimate for the reduced spreading pressure has been calculated, then the pure component pressures can be calculated using Equation 16.

With the pure component pressures, the hypothetical amount adsorbed for each component can be calculated using the pure component isotherm equation, such as the Langmuir isotherm equation in Equation 17.

Once the hypothetical adsorbed amount for each component has been determined, then the Newton-Raphson equations can be used. The Newton-Raphson equation for iterating the reduced spreading pressure that will be used is

$$z^{(k+1)} = z^{(k)} - \frac{F(z^{(k)})}{F'(z^{(k)})} \tag{21}$$

where $z^{(k)}$ is the reduced spreading pressure at the current iteration, $z^{(k+1)}$ is the reduced spreading pressure for the next iteration, and $F(z^{(k)})$ & $F'(z^{(k)})$ are the function of and the derivative of the function of the current reduced spreading pressure, respectively. The equation for $F(z^{(k)})$ can be written as (Do, 1998)

$$F(z^{(k)}) = \sum_{i=1}^{N} \frac{Py_i}{P_i^0(z^{(k)})} - 1 \tag{22}$$

and the equation for $F'(z^{(k)})$ can be written as

$$F'(z^{(k)}) = -\sum_{i=1}^{N} \frac{Py_i}{P_i^0(z^{(k)})C_{\mu i}^0} \tag{23}$$

where the summations are done across all of the adsorbed components. After calculating $z^{(k+1)}$ using Equation 21, the absolute value of the difference between $z^{(k+1)}$ and $z^{(k)}$ is calculated and compared to the preset tolerance value. If the absolute value of the difference between the two reduced spreading pressures is higher than the tolerance, $z^{(k)}$ will be set to the value of $z^{(k+1)}$ and the new $z^{(k)}$ will be used to go through the sequence

of calculations again beginning with calculating the pure component pressures using Equation 16, all the way through using the Newton-Raphson method to calculate a new $z^{(k+1)}$. The same tolerance comparison will then be performed, and a while loop will continue iterating through those same steps until the final value is within the tolerance.

After the first while loop has concluded with the value of the reduced spreading pressure having converged to the final value, the process of calculating the actual predicted adsorbed concentration and mole fraction for each component can then begin. The first step in this process is again calculating the pure component pressures using Equation 16.

Using the pure component pressures, the adsorbed phase mole fractions and hypothetical adsorbed concentrations for each component can be calculated. Adsorbed phase mole fractions are calculated using Equation 14 and the hypothetical adsorbed concentrations are calculated using the pure component isotherm equation of choice, so in the case of the Langmuir isotherm equation, Equation 17.

With the adsorbed phase mole fractions and hypothetical adsorbed concentrations of each component known, the total adsorbed concentration can then be calculated using Equation 18.

From the total adsorbed concentration and the adsorbed phase mole fractions for each component, the actual adsorbed concentration for each component can then be calculated using Equation 19. The actual adsorbed concentrations of each component and the total pressure are then stored for use later with data analysis.

The selectivity of the adsorbed components of interest can then be calculated using the commonly used adsorption selectivity equation, which is written as (Principe & Fletcher, 2020)

$$s_{1,2} = \frac{x_1/y_1}{x_2/y_2} \tag{24}$$

where $s_{1,2}$ is the selectivity of the two desired components, x_i is the adsorbed phase mole fraction of component i, and y_i is the gas phase mole fraction of species i. Any number of selectivities can be calculated, depending on user inputs. The selectivity is then stored for later use.

After all the calculations starting with calculating an initial estimate for the reduced spreading pressure have been performed for the current total pressure, a for loop then performs those calculations again for all the total pressures specified by the user. Once this for loop terminates, the resulting data is the actual adsorbed concentration of each component at all of the total pressures and the desired selectivities of interest at all of the total pressures.

After the termination of the for loop in the previous step, the adsorbed concentration of each component and the desired selectivities are written to a .csv file named ‘results.csv’ along with their corresponding total pressures for use in external data analysis software, such as Microsoft Excel.

The code then also plots the adsorbed concentration of each component as a function of pressure on one figure and the desired selectivities as a function of pressure in a second figure for quick visual analysis. Once the generated plots are closed, the code then terminates.

CHAPTER 5

RESULTS & DISCUSSION

Code Validation

Prior to generating novel mixed gas adsorption equilibrium data, it is important to first verify that the accuracy of the code is sufficient for a wide range of sorbents and gases, or to at least understand its limitations. In this thesis, the code was validated using experimental data for binary, ternary, and quaternary adsorption equilibrium. Although the code as written is designed to handle any number of components, comparing the generated predictions to data for mixed gas adsorption with anywhere from two to four components should provide a comprehensive and reasonable assessment of the code.

The first mixed-gas adsorption equilibrium experimental data used for comparison was that of binary mixtures. The first binary mixture analyzed was for ethane (C_2H_6) and methane (CH_4) being adsorbed onto a commercially available heterogeneous activated carbon sorbent manufactured by the Pittsburgh Chemical Company (Reich et al., 1980). The component and total loadings are plotted below in Figure 6 as functions of the total pressure. The initial molar composition of the gas stream is 50.1% C_2H_6 and 49.9% CH_4, and measurements were taken at 212.7 K.

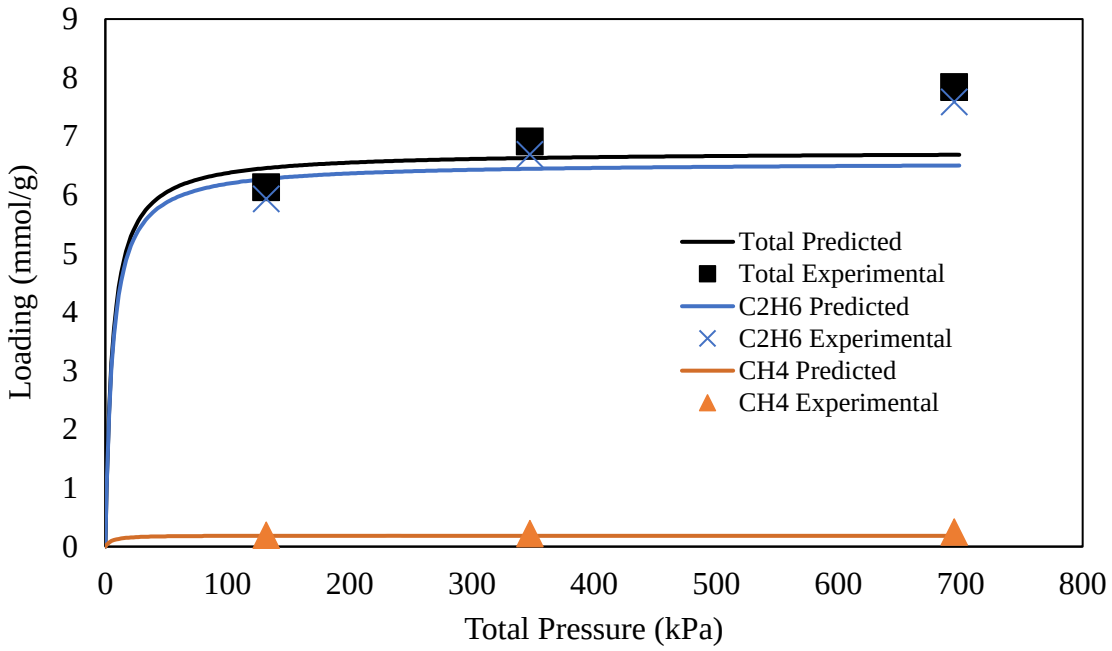

Figure 6: Adsorption Loadings (mmol/g) as a Function of Total Pressure (kPa) for a Mixture of C_2H_6 and CH_4 Adsorbed onto an Activated Carbon

Figure 6 shows the loadings predicted by the code developed for this thesis as solid line data series, with the experimentally observed loadings shown as points without lines. The colors correspond to the component. In Figure 6, the component loadings predicted by the code are relatively close to the experimentally observed loadings for pressures up to 350 kPa. At total pressures greater than 350 kPa, the predicted loadings begin to diverge significantly from the actual experimental values, with the experimental value of the total loading at 700 kPa being 17.3% higher than the predicted value.

The second binary mixture analyzed was for propane (C_3H_8) and carbon dioxide (CO_2) being adsorbed onto a zeolite, specifically H-Mordenite (Talu & Zwiebel, 1986). The component and total loadings are plotted below in Figure 7 as functions of the total pressure. The initial molar composition of the gas stream is 16.7% CO_2 and 83.3% C_3H_8, and measurements were taken at 303.15 K.

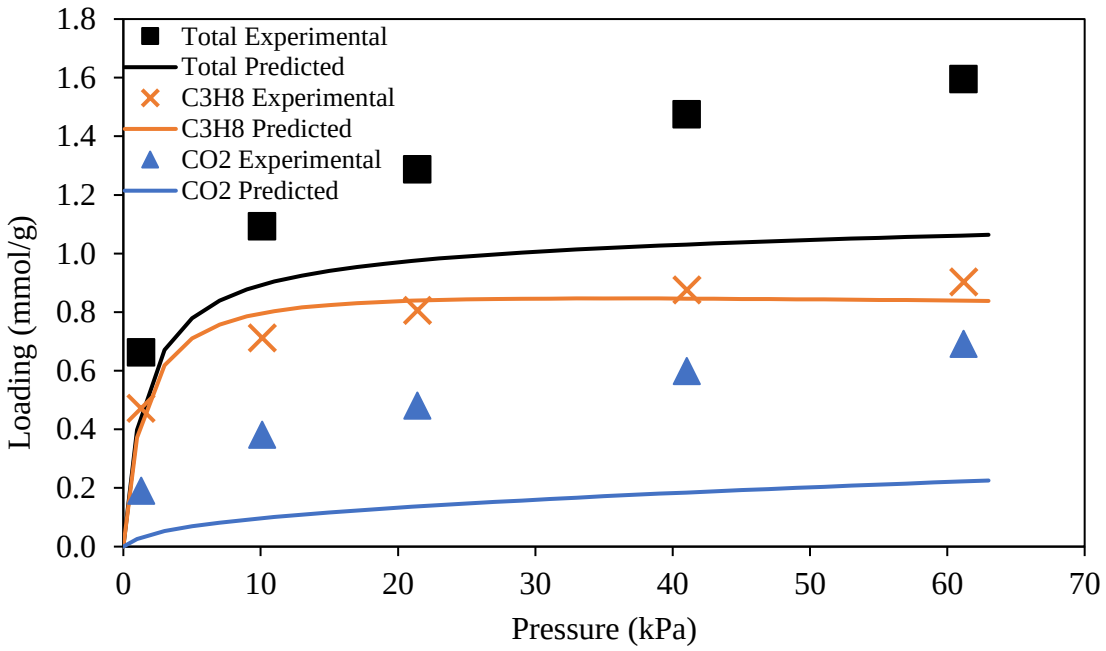

Figure 7: Adsorbed Loadings (mmol/g) as a Function of Total Pressure (kPa) for a Mixture of CO_2 and C_3H_8 onto H-Mordenite

From Figure 7, it is immediately clear that the loadings predicted by the code are far less accurate than in the previous binary mixture example. Specifically, the predicted loading of CO_2 is significantly less than was observed experimentally, which results in a large deviation in the total loading amount as well. The predicted loading of C_3H_8 is relatively accurate for the pressure range that experimental data was provided for, though it would likely deviate much more from the model's predicted loading at higher pressures based on visual analysis of the trends for both the experimental and predicted data.

Moving onto ternary gas mixtures, the only ternary mixture analyzed was CO_2, CH_4, and nitrogen (N_2) being adsorbed onto a zeolite of type 13X (Avijegon et al., 2018). The component and total loadings are plotted below in Figure 8 as functions of the total pressure. The initial molar composition of the gas stream is 56% CO_2, 19% N_2, and 25% CH_4, and measurements were taken at 303 K.

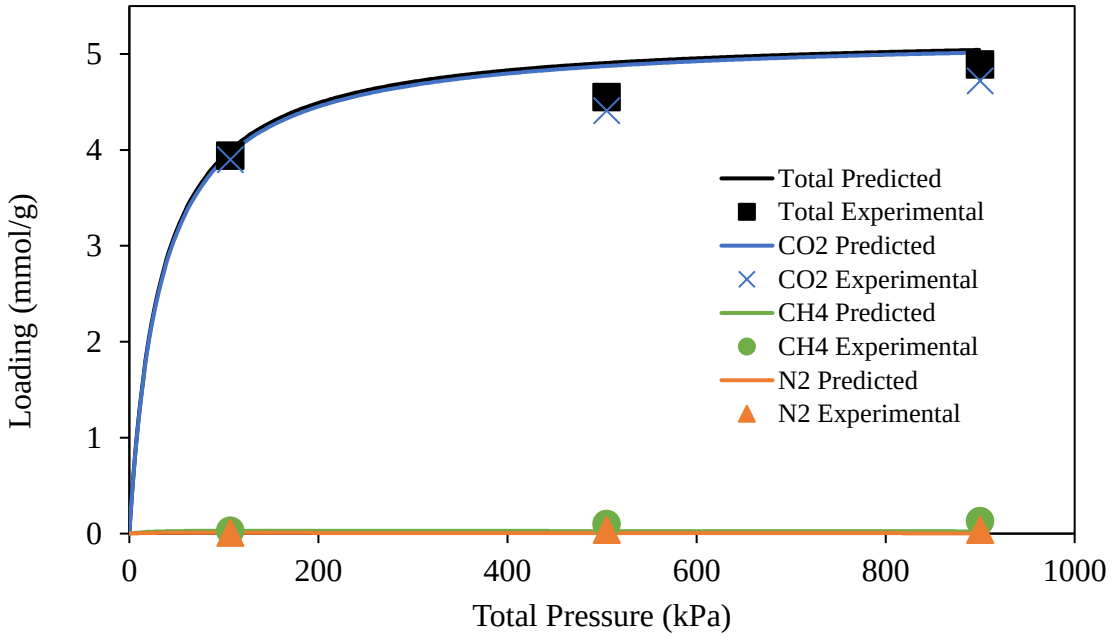

Figure 8: Adsorbed Loadings (mmol/g) as a Function of Total Pressure (kPa) for a Mixture of CO_2, N_2, and CH_4 onto a Type 13X Zeolite

By looking at Figure 8, it can be observed that the predicted loadings are relatively close across a wide range of pressures. Specifically at the lowest and highest experimental data points, the predicted loadings are almost exactly the same as the experimental loadings. The experimental point at ~500 kPa is further from the predicted value than the other experimental points but is still within a reasonable range of the prediction.

For the quaternary gas mixtures, there are three sets of experimental data that will be compared to model predictions. The first quaternary mixture analyzed was for CO_2, CH_4, N_2, and hydrogen (H_2) being adsorbed onto an activated carbon adsorbent of type Norit R1 (Rother & Fieback, 2013). The component and total loadings are plotted below in Figure 9 as functions of the total pressure. The initial molar composition of the gas

stream is 33% CO_2, 60% CH_4, 5% N_2, and 2% H_2, and measurements were taken at 298 K.

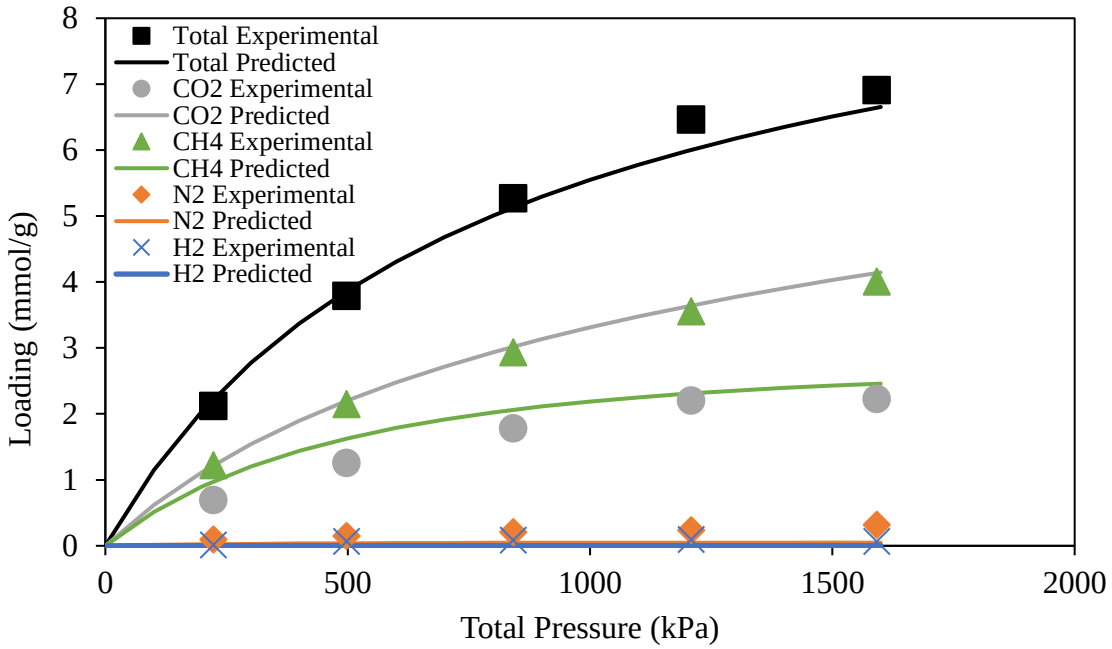

Figure 9: Adsorbed Loadings (mmol/g) as a Function of Total Pressure (kPa) for a Mixture of CO_2, CH_4, N_2, and H_2 onto a Type Norit R1 Activated Carbon Adsorbent

The predicted values for total loading and H_2 loading in Figure 9 are extremely close to the observed experimental values across a huge range of pressures up to 1600 kPa. However, the predicted loadings of CH_4, CO_2, and N_2 are far off from their exact values. An interesting note about Figure 9 is that the predicted CO_2 and CH_4 loadings are almost exactly reversed from what the experimental data shows they should be.

The second quaternary mixture analyzed was for CO_2, CH_4, N_2, and H_2 being adsorbed onto a MOF, Basolite C300 (Rother & Fieback, 2013). The component and total loadings are plotted below in Figure 10 as functions of the total pressure. The initial molar composition of the gas stream is 33% CO_2, 60% CH_4, 5% N_2, and 2% H_2, and measurements were taken at 298 K.

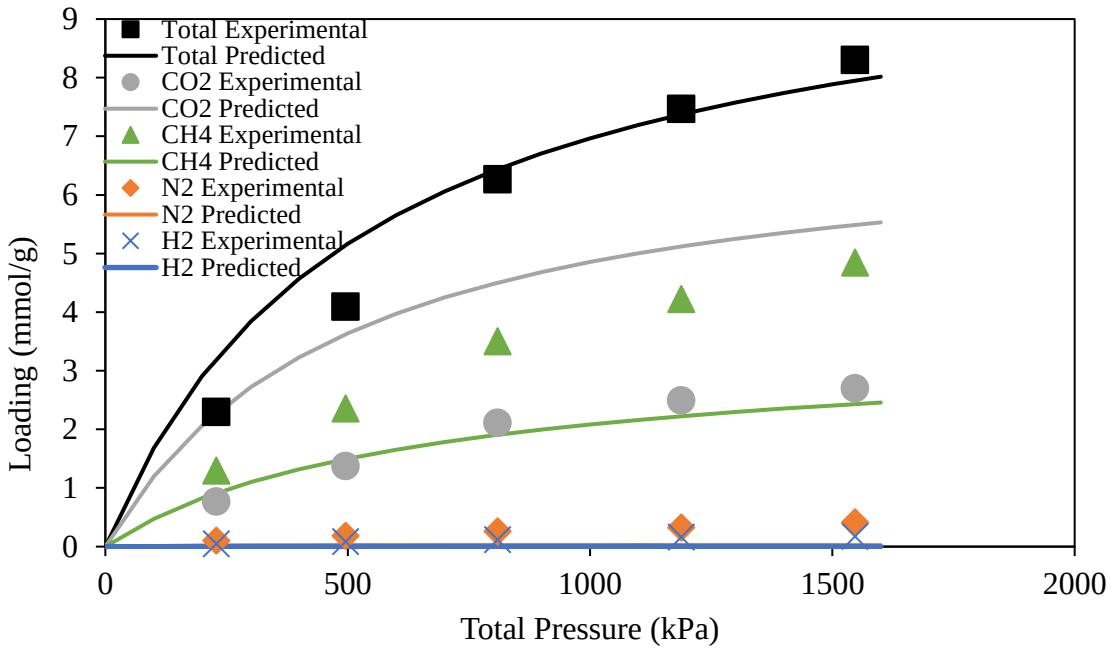

Figure 10: Adsorbed Loadings (mmol/g) as a Function of Total Pressure (kPa) for a Mixture of CO_2, CH_4, N_2, and H_2 onto Basolite C300

Similar to Figure 9, the predicted values for total loading and H2 loading in Figure 10 are relatively accurate at the pressures shown. The predicted total loading values are less accurate when compared to those in Figure 9, but they are still relatively accurate calculations, especially for pressures greater than 750 kPa. The predicted CO_2 loading in Figure 10 is much higher than the observed experimental values and the predicted CH_4 values are much lower than the experimental values.

The third ternary mixture analyzed was for CO_2, CH_4, N_2, and H_2 being adsorbed onto a type 13X zeolite (Rother & Fieback, 2013). The component and total loadings are plotted below in Figure 11 as functions of the total pressure. The initial molar composition of the gas stream is 33% CO_2, 60% CH_4, 5% N_2, and 2% H_2, and measurements were taken at 298 K.

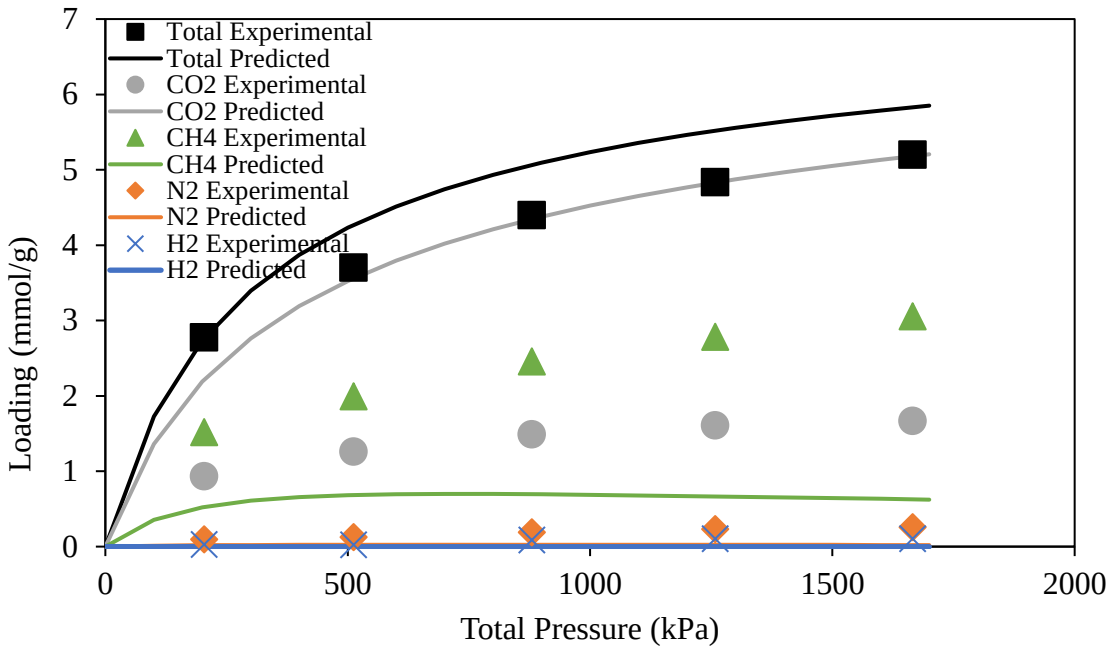

Figure 11: Adsorbed Loadings (mmol/g) as a Function of Total Pressure (kPa) for a Mixture of CO_2, CH_4, N_2, and H_2 onto Zeolite 13X

The problems noticed in the predicted values shown in Figures 9 and 10 are also present in Figure 11, and they are much more prominent than in either of the previous figures. The predicted loading of CO_2 is extremely high compared to the experimental data, with the predicted loading of CH_4 being too low. The predicted values in Figure 11 are a much worse prediction of the component and total loadings than in Figure 9 or 10. The only predicted loading values close to their corresponding experimental values are those of the total loading, although even those are further off than the previous two quaternary examples.

Flue Gas Condition Simulations

Although the developed code can be applied to any system which pure gas isotherms have been obtained for, the gas streams that are of the most interest in this

thesis are for carbon capture, as discussed earlier. As such, the first application conditions for which multicomponent equilibrium data was generated were for a humid flue gas stream from a coal-fired power plant. A typical molar composition for flue gas streams of this type is 13% CO_2, 76% N_2, and 11% water (H_2O) (*Flue Gas Properties Table*, n.d.). The temperature in both simulated cases was 298 K.

The first of the two adsorbents looked at under flue gas conditions was a magnesium-based MOF referred to as Mg-MOF-74 (A. Mason et al., 2011; Ben-Mansour et al., 2018). A plot of the predicted component loadings as a function of pressure is shown below in Figure 12.

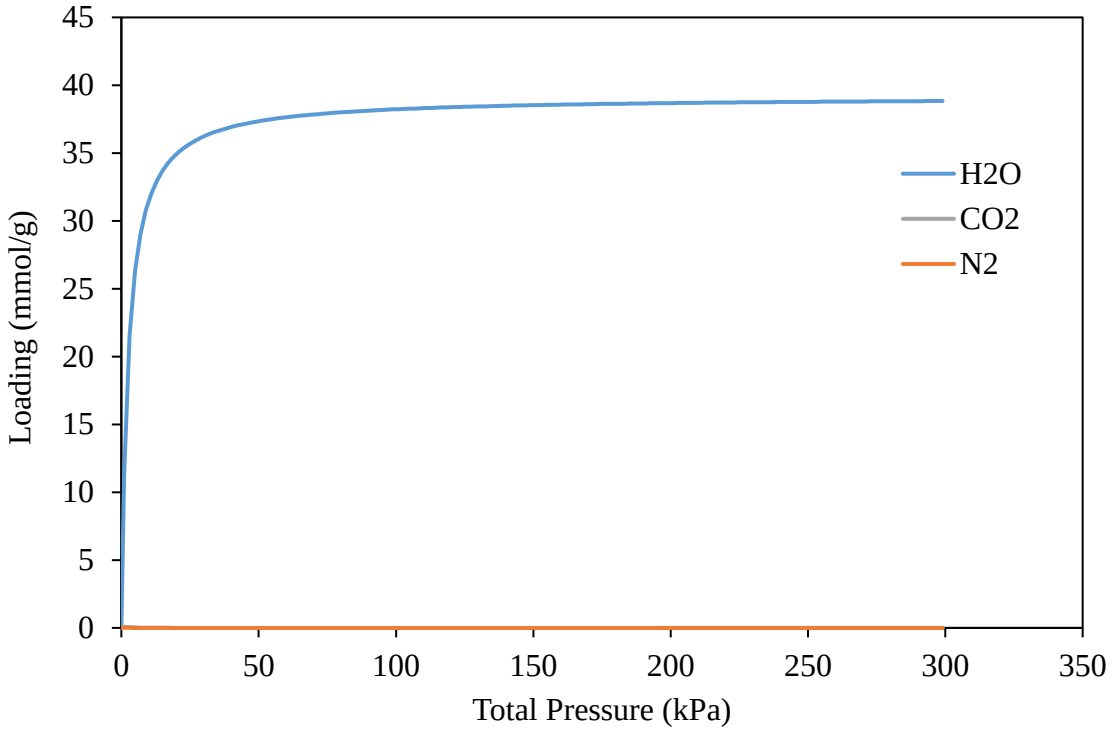

Figure 12: Adsorbed Loadings (mmol/g) as a Function of Total Pressure (kPa) for Flue Gas Conditions on Mg-MOF-74

The most evident trend in Figure 12 is that the H_2O dominates the CO_2 and N_2 in the predicted loadings. Of the CO_2 and the N_2, only the CO_2 is ever adsorbed in a large

enough amount to appear as a nonzero loading in Figure 12, which happens briefly at pressures less than 10 kPa. This can be seen more clearly in the semilog plot shown below in Figure 13, which shows the same data as Figure 12 but the y-axis is a logarithmic scale instead of a linear scale.

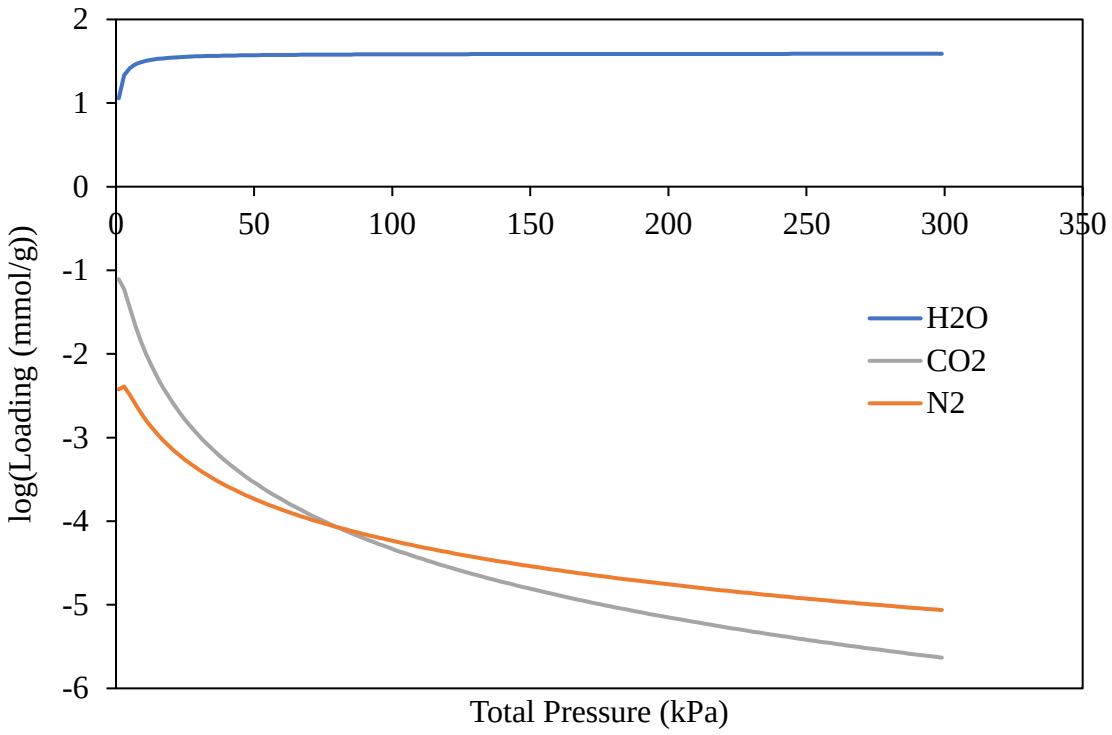

Figure 13: Semilog Plot of Adsorbed Loadings (mmol/g) as a Function of Total Pressure (kPa) for Flue Gas Conditions on Mg-MOF-74

Figure 13 shows both CO_2 and N_2 adsorb far less than H_2O, and in addition, CO_2 is adsorbed less than N_2 at pressures higher than 80 kPa.

Since CO_2/N_2 selectivity is such a commonly used metric for adsorbents in carbon capture, the CO_2/N_2 selectivity is plotted as a function of total pressure below in Figure 14.

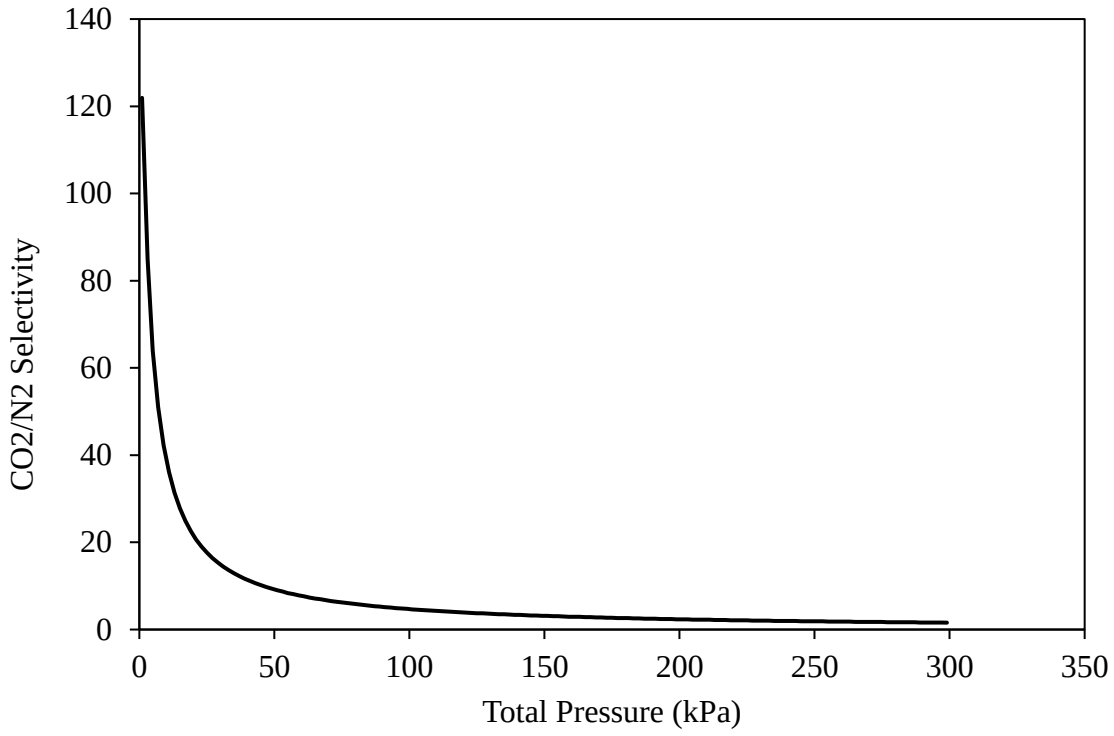

Figure 14: CO_2/N_2 Selectivity as a Function of Total Pressure (kPa) for Flue Gas Conditions on Mg-MOF-74

Looking at Figures 13 and 14, the CO_2 adsorption clearly starts much higher than that of the N_2, but as the pressure gets higher and more H_2O is adsorbed, the loadings for both CO_2 and N_2 decrease to both be very low. This results in CO_2/N_2 selectivity values that are close to 1 at pressures higher than 80 kPa.

The second adsorbent looked at under flue gas conditions was a type 13X zeolite, referred to as Zeolite 13X (Ben-Mansour et al., 2018; Cavenati et al., 2004). A plot of the predicted component loadings as a function of pressure is shown below in Figure 15.

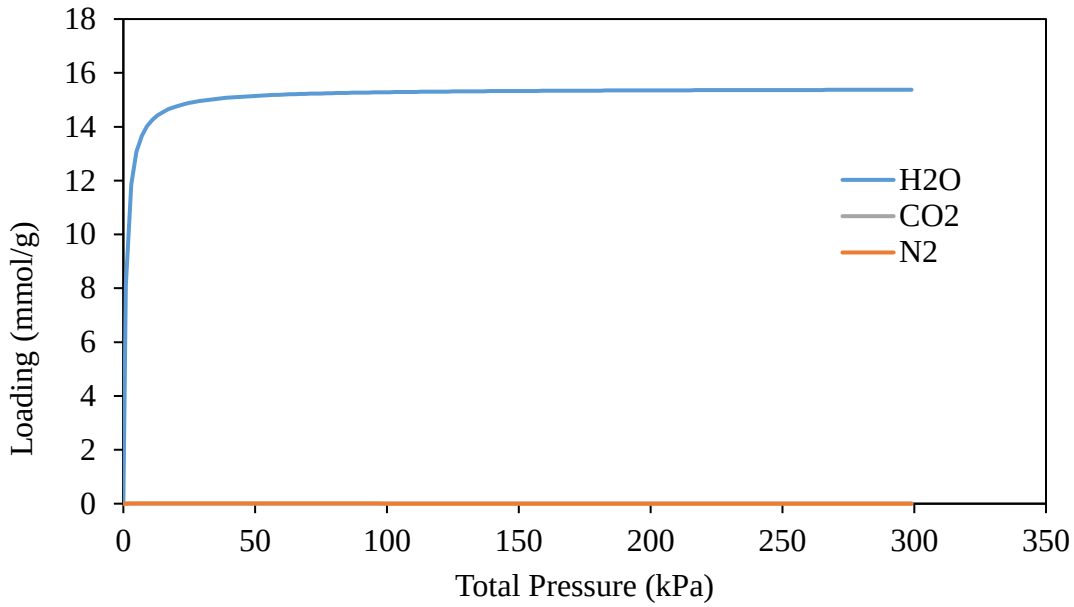

Figure 15: Adsorbed Loadings (mmol/g) as a Function of Total Pressure (kPa) for Flue Gas Conditions on Zeolite 13X

Similar to the same gas mixture being adsorbed onto the Mg-MOF-74, it is clear from Figure 15 that the H_2O dominates the CO_2 and N_2 in the predicted loadings. One small difference between the Mg-MOF-74 and the Zeolite 13X in terms of their component loadings is the Zeolite 13X never adsorbs the CO_2 strongly enough for it to show up and be visually distinguishable from the N_2 loading in Figure 15. To identify small differences in adsorption between CO_2 and N_2, a semilog plot is shown below in Figure 16.

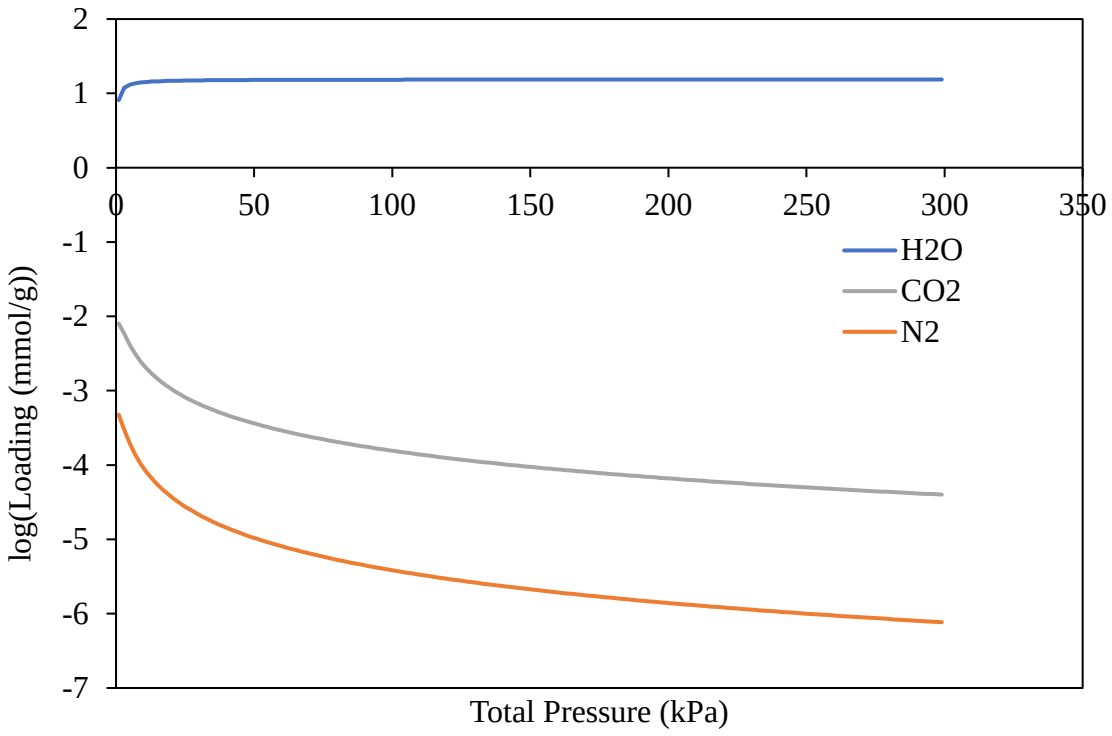

Figure 16: Semilog Plot of Adsorbed Loadings (mmol/g) as a Function of Total Pressure (kPa) for Flue Gas Conditions on Zeolite 13X

Figure 16 shows that although the loadings of both CO_2 and N_2 are extremely low, the CO_2 is adsorbed significantly more strongly than the N_2. The CO_2/N_2 selectivity will also again be used to analyze differences in adsorption for CO_2 and N_2. The CO_2/N_2 selectivity is plotted as a function of total pressure below in Figure 17.

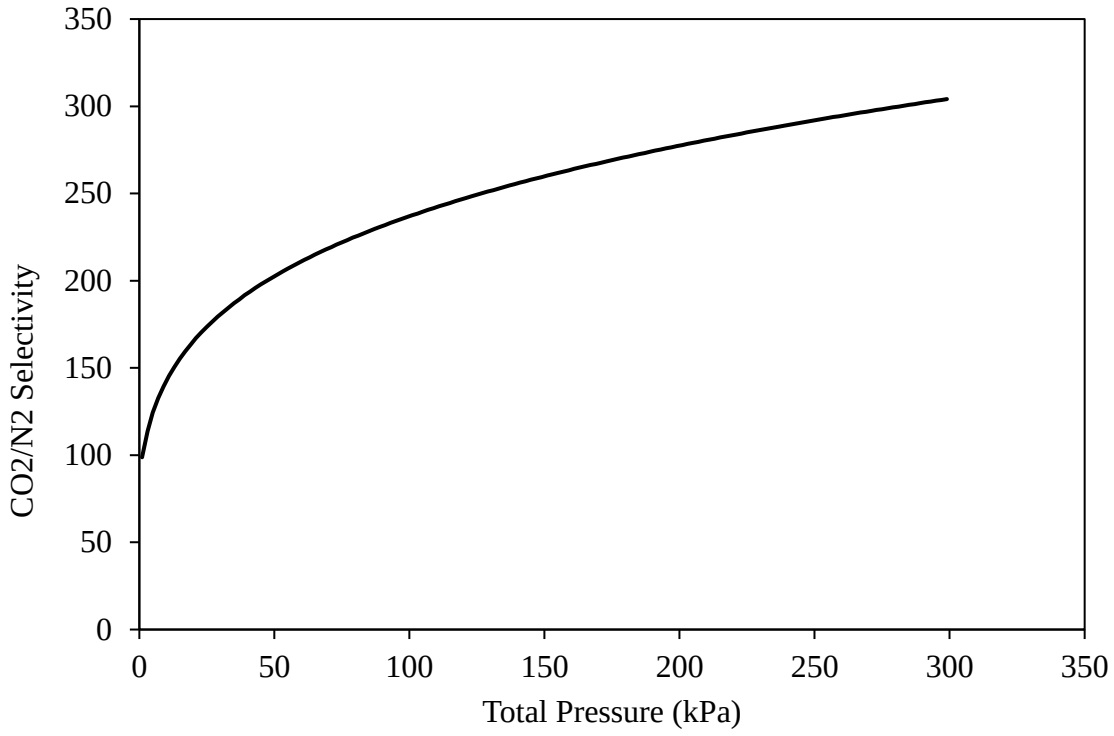

Figure 17: CO_2/N_2 Selectivity as a Function of Total Pressure (kPa) for Flue Gas Conditions on Zeolite 13X

Figure 17 shows the CO_2/N_2 selectivity continually increasing as the total pressure increases. This is the opposite of the trend seen for the Mg-MOF-74 and indicates that utilizing high pressures for flue gas adsorption would be optimal if using this Zeolite 13X. However, the overall loadings are still extremely low, and as such, it would make a relatively inefficient adsorbent under the given flue gas conditions.

Industrial Natural Gas Process Condition Simulations

The second set of application conditions is for one of many industrial natural gas processes. The particular set of conditions analyzed in this thesis is for purifying a nitrogen gas stream such that it is pure enough to meet natural gas pipeline specifications. A typical inlet molar concentration for a natural gas pipeline purification process is 40%

CO_2, 30% N_2, and 30% CH_4 (Watson et al., 2012). These molar concentrations will be the ones used for the simulated mixed gas equilibrium results of both adsorbents at a temperature of 298 K.

The first adsorbent analyzed with natural gas purification conditions was a type 13X zeolite, referred to as Zeolite 13X (Park et al., 2016). A plot of the predicted component loadings as a function of pressure is shown below in Figure 18.

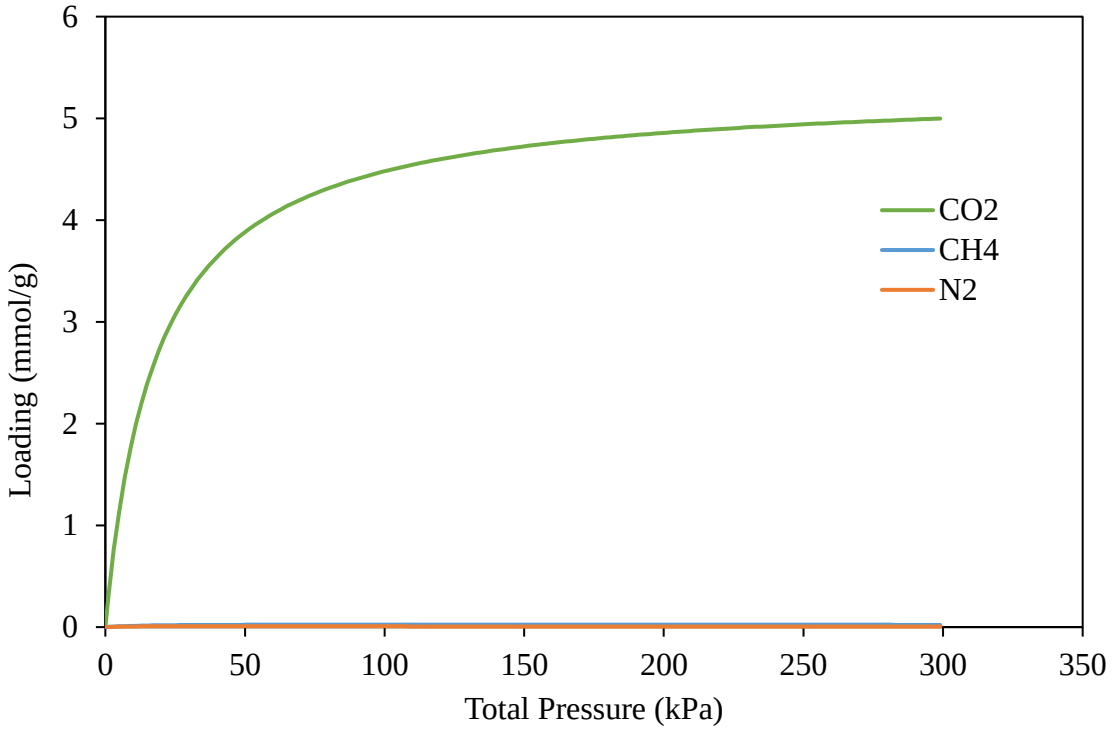

Figure 18: Adsorbed Loadings (mmol/g) as a Function of Total Pressure (kPa) for Natural Gas Purification Conditions on Zeolite 13X

From Figure 18 the Zeolite 13X clearly adsorbs CO_2 much more readily than either the CH_4 or the N_2, which makes it a strong potential candidate for use in natural gas purification processes for CO_2 removal. However, the Zeolite 13X is less efficient at adsorbing the N_2. This means that for use in natural gas purification, the Zeolite 13X would likely be only one part of a multistep process, whereas the other step would need

to selectively adsorb the N_2 much more strongly. At pressures greater than 200 kPa, the Zeolite 13X also starts to adsorb CH_4 more strongly than N_2, which could be an issue since that would result in the effluent stream becoming less pure than if the Zeolite 13X was used at less than 200 kPa. To determine adsorption differences between the CH_4 and N_2, a semilog plot was constructed and is shown below in Figure 19.

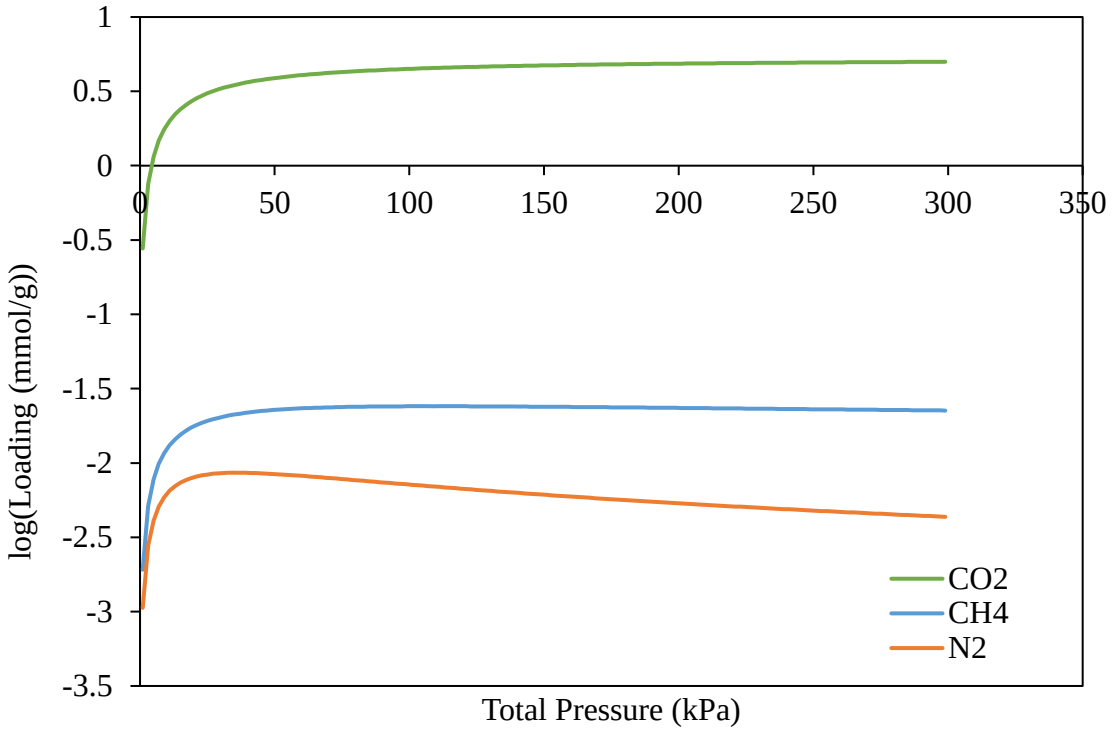

Figure 19: Semilog Plot of Adsorbed Loadings (mmol/g) as a Function of Total Pressure (kPa) for Natural Gas Purification Conditions on Zeolite 13X

Figure 19 shows the CH_4 is adsorbed more strongly than the N_2, and both gases are adsorbed most at 40-80 kPa. The loadings for both gases then begin to decrease at higher pressures.

The second adsorbent analyzed with natural gas purification conditions was a chromium-based MOF, referred to as MIL-101 (Zhang et al., 2015). A plot of the predicted component loadings as a function of pressure is shown below in Figure 20.

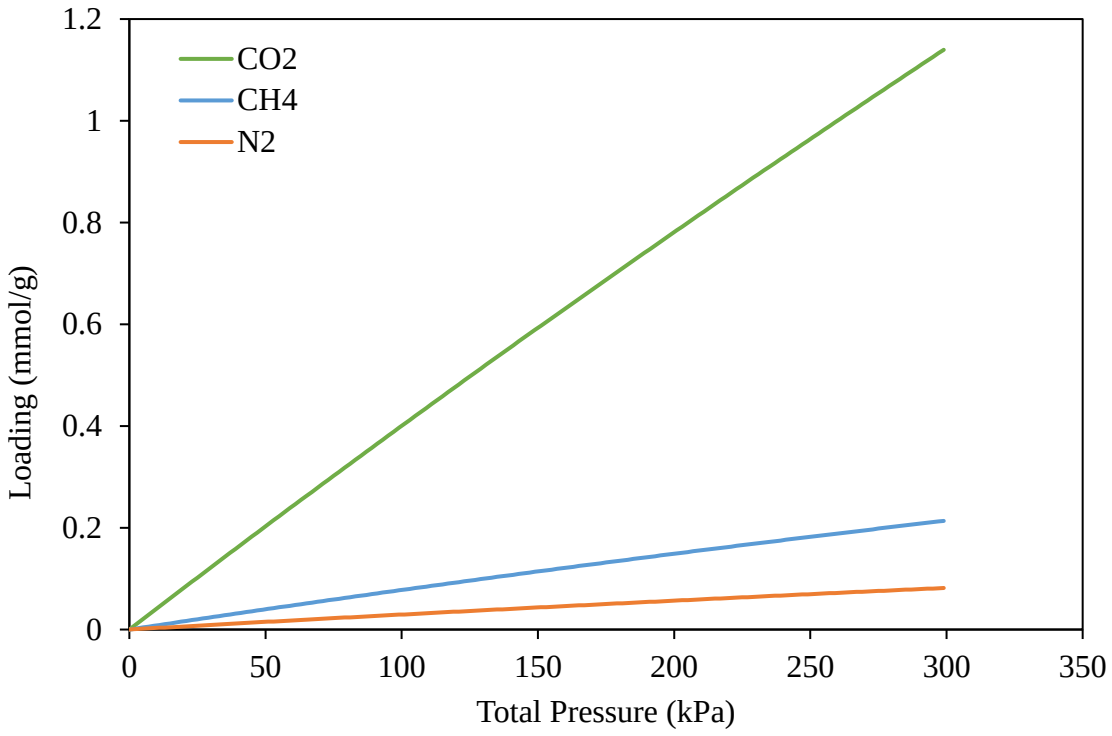

Figure 20: Adsorbed Loadings (mmol/g) as a Function of Total Pressure (kPa) for Natural Gas Purification Conditions on MIL-101

The loading behavior for MIL-101 shown in Figure 20 is very different from that of Zeolite 13X in Figure 18. In Figure 20, all three components show a nearly linear increase in loading with an increase in pressure. The CO_2 loading is still by far the strongest, but the CH_4 and N_2 loadings are distinguishable from one another, which was not the case using the Zeolite 13X. One issue with using MIL-101 for natural gas purification processes is that it adsorbs CH_4 approximately twice as strongly as N_2, meaning that using it would result in an effluent stream with a lower CH_4 to N_2 ratio than when it was initially fed in. A semilog plot of adsorbed amounts is shown below in Figure 21 to more easily distinguish between the components.

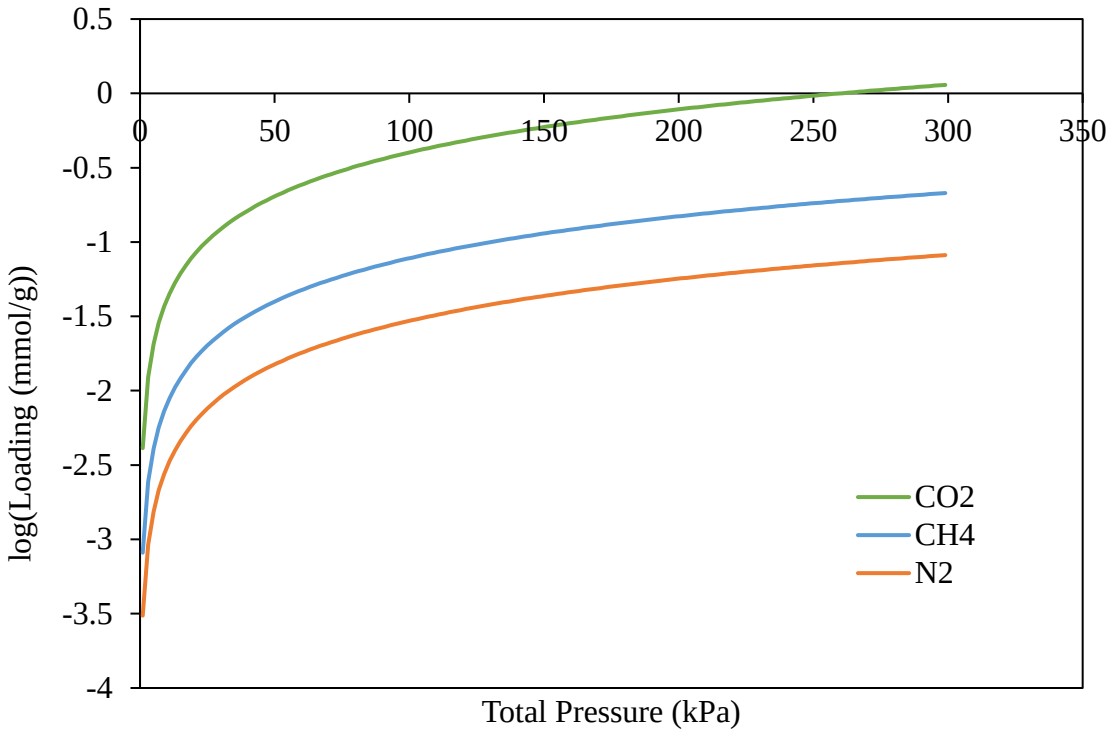

Figure 21: Semilog Plot of Adsorbed Loadings (mmol/g) as a Function of Total Pressure (kPa) for Natural Gas Purification Conditions on MIL-101

Figure 21 shows the trends discussed previously more clearly, with the CO2 being adsorbed the strongest, and then CH_4 and N_2 both being adsorbed an order of magnitude less.

Hydrogen Gas Purification Condition Simulations

The final set of application conditions is for H_2 gas production by reforming natural gas, as this is one of the two most utilized methods to produce H_2, alongside H_2O electrolysis (*Hydrogen Production*, n.d.). When performing pressure swing adsorption for H_2 purification, a typical inlet molar concentration is 5% carbon monoxide (CO), 15% CO_2, 5% CH_4, and 75% H_2 (Al-Naddaf et al., 2020). These are the molar concentrations that will be used to analyze the two selected adsorbents at a temperature of 298 K.

The first sorbent analyzed with H_2 purification conditions was a type 5A zeolite, referred to as Zeolite 5A (Al-Naddaf et al., 2020; Pakseresht et al., 2002). A plot of the predicted component loadings as a function of pressure is shown below in Figure 22.

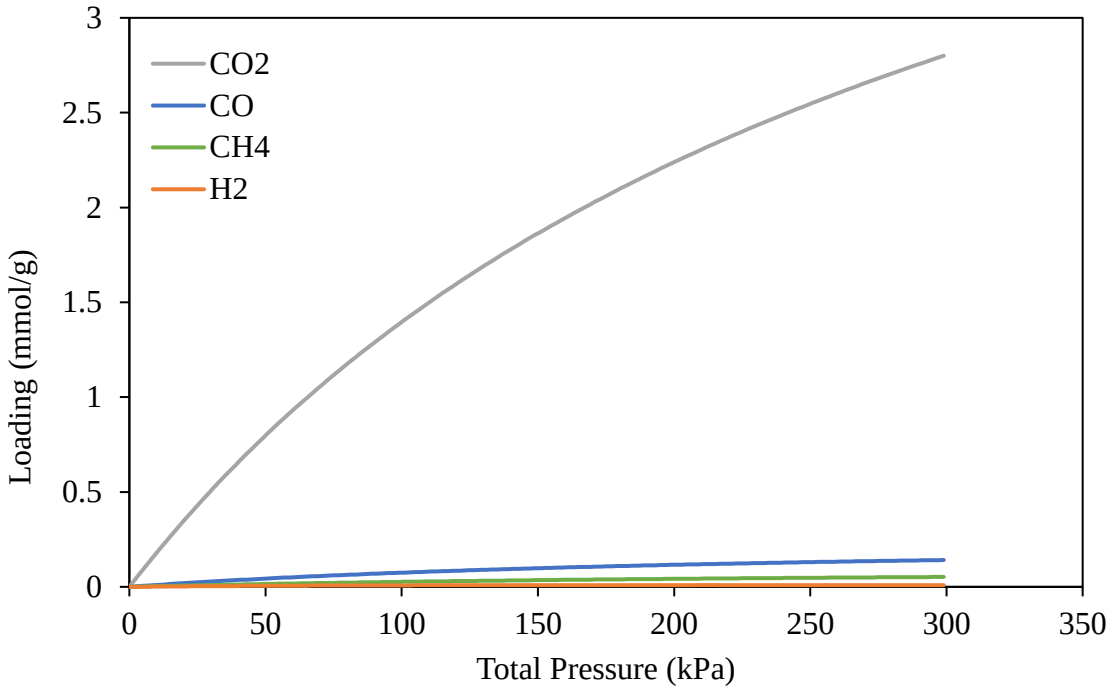

Figure 22: Adsorbed Loadings (mmol/g) as a Function of Total Pressure (kPa) for H_2 Gas Purification Conditions on Zeolite 5A

As is shown in Figure 22, the CO_2 is adsorbed much more strongly than the other components. However, the loadings for the other three components are all distinguishable from one another. To distinguish between the three lesser adsorbed components, a semilog plot is shown below in Figure 23.

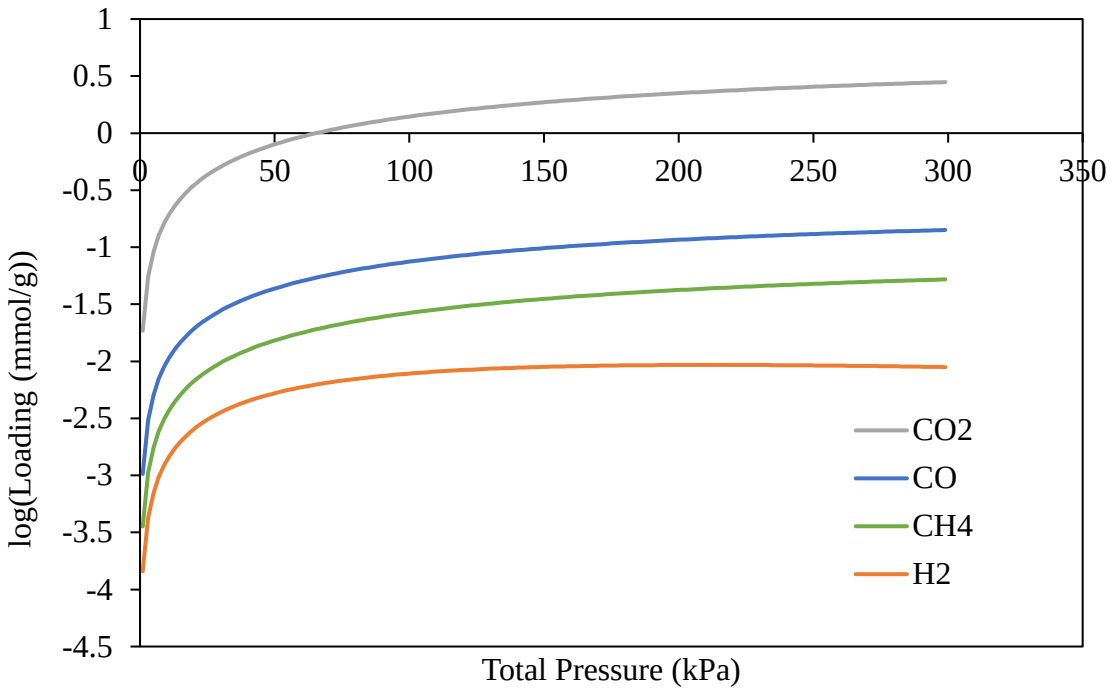

Figure 23: Semilog Plot of Adsorbed Loadings (mmol/g) as a Function of Total Pressure (kPa) for H_2 Gas Purification Conditions on Zeolite 5A

Looking at Figure 23, the component which clearly has the lowest loading is the H_2. Due to this, the Zeolite 5A would make a very good sorbent for use in a multistage H_2 gas purification process. The effluent stream from a packed bed full of this Zeolite 5A would contain very little CO_2, most of the CO, most of the CH_4, and almost all the H_2. This gas stream could then be directed through packed beds full of other adsorbents which selectively adsorb CO and CH_4 much more strongly than H_2.

The second adsorbent analyzed with H_2 purification conditions was a coal-derived activated carbon, referred to as CD-AC (Park et al., 2014). A plot of the predicted component loadings as a function of pressure is shown below in Figure 24.

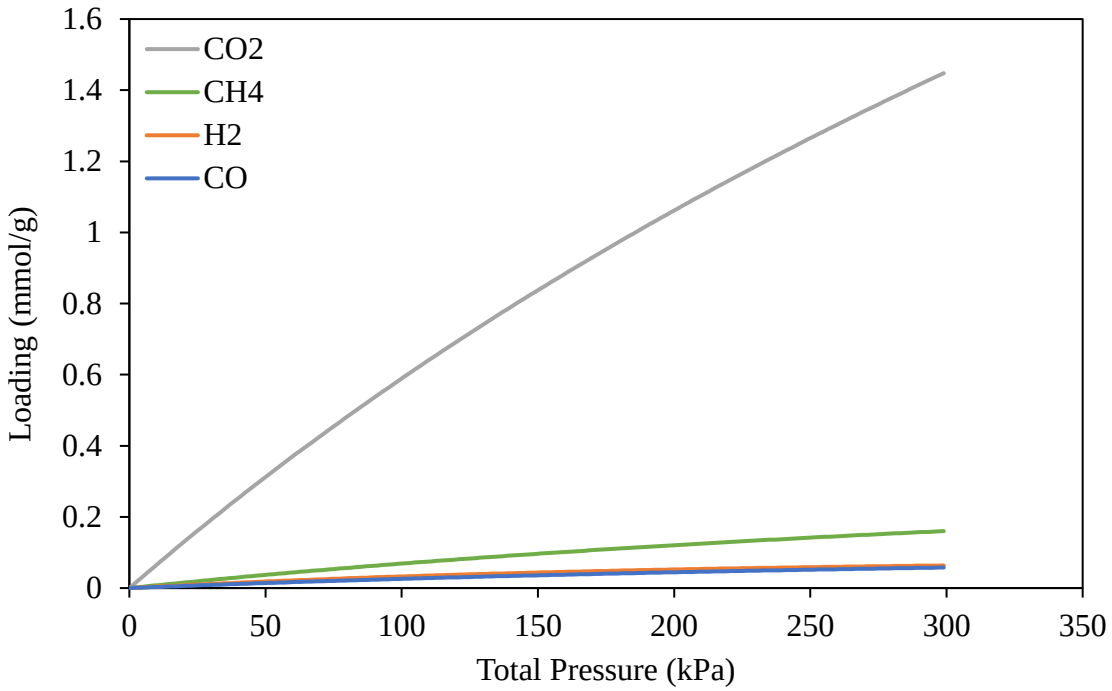

Figure 24: Adsorbed Loadings (mmol/g) as a Function of Total Pressure (kPa) for H_2 Gas Purification Conditions on CD-AC

Looking at Figure 24, the CO_2 is adsorbed much less strongly overall and in relation to the other components when compared to Figure 22. To distinguish component loadings from one another more, a semilog plot is shown below in Figure 25.

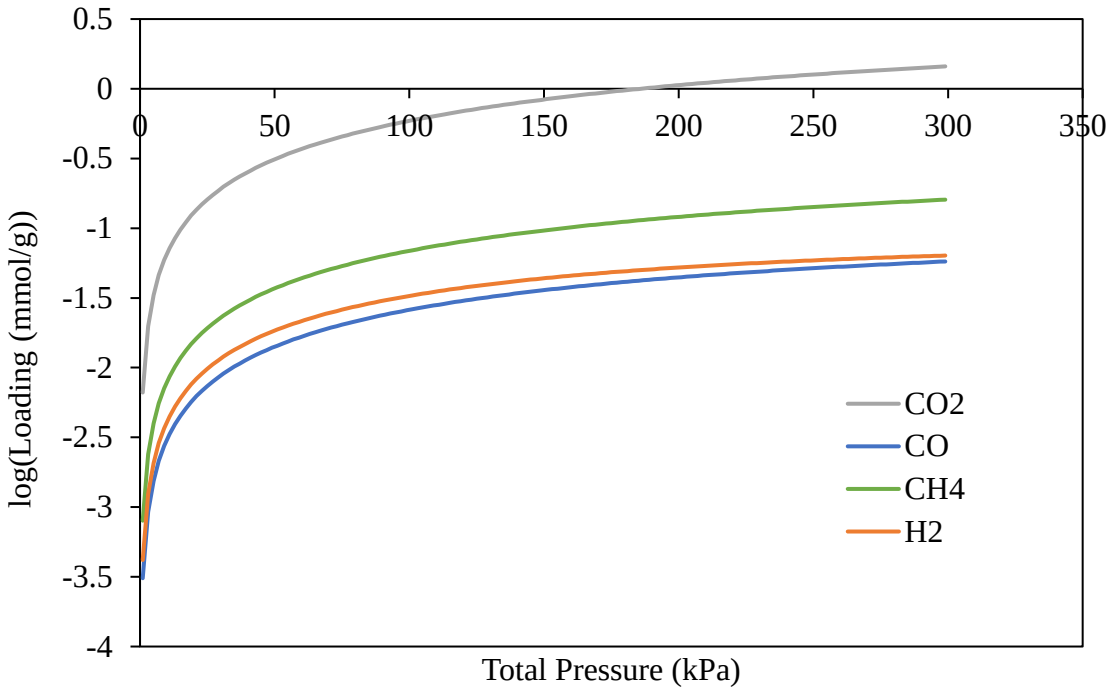

Figure 25: Semilog Plot of Adsorbed Loadings (mmol/g) as a Function of Total Pressure (kPa) for H_2 Gas Purification Conditions on CD-AC

As can be observed from Figure 25, the CD-AC adsorbs much more H_2 relative to the other components when compared to the Zeolite 5A in Figure 23. This means that when purifying an H_2 gas stream, there would be less H_2 left in the effluent gas after being flowed through a packed bed filled with CD-AC than through a bed filled with Zeolite 5A. However, despite those relative shortcomings, CD-AC could still be a viable part of a multistage H_2 gas purification process, much like Zeolite 5A.

CHAPTER 6

CONCLUSION

The goal of this thesis was to develop code that could be used to accurately simulate multicomponent adsorption equilibrium data when provided with isotherm equation parameters or pure gas adsorption equilibrium data. Once developed, the code was then used to analyze multiple sorbents for three sets of gas conditions of interest. Those three sets of conditions were for carbon capture from a flue gas stream, methane recovery from a contaminated natural gas stream, and hydrogen gas purification from reforming natural gas.

When looking at the generated results for flue gas streams, the main takeaway is that for the sorbents analyzed, H_2O was easily the most adsorbed component. H_2O was adsorbed so strongly that it essentially negated any adsorption of either the N_2 or CO_2. This means that in a humid environment such as one with conditions similar to those used for the predictions, neither the Mg-MOF-74 nor the Zeolite 13X will capture CO_2 in a satisfactory amount. Due to their high affinities for H_2O adsorption, neither adsorbent should be deployed for use in humid flue gas conditions.

The generated results for contaminated natural gas conditions were very different between the two sorbents, Zeolite 13X and MIL-101. Although both sorbents adsorbed CO_2 much more strongly than either the CH_4 or N_2, the magnitude of CO_2 adsorbed was almost 6 times greater for the Zeolite 13X than the MIL-101. This means that for a given amount of sorbent, the Zeolite 13X will adsorb much more CO_2 before becoming saturated. Additionally, the MIL-101 had much lower selectivity of CO_2 in relation to the other components than the Zeolite 13X, with the MIL-101 adsorbing significant amounts

of both CH_4 and N_2. If designing a natural gas purification process, Zeolite 13X would overall be a much better sorbent to select due to the previously mentioned factors. However, Zeolite 13X would have to be only one stage of a multistage process for purifying natural gas streams, since it adsorbed essentially none of the N_2, meaning the effluent stream after a packed bed with Zeolite 13X would still have almost all of the N_2 and CH_4 in it, instead of the desired result of a pure stream comprised mainly of CH_4.

When analyzing the generated results for hydrogen gas purification from reforming natural gas, the two sorbents had interesting similarities and differences. One main similarity is that both the Zeolite 5A and the CD-AC adsorbed CO_2 much more strongly than any other component, meaning both sorbents could be used in a hydrogen gas purification process to remove the CO_2 present. However, one major difference is that the Zeolite 5A adsorbs H_2 far worse than CD-AC while having overall much higher saturation loadings in general. This means that more Zeolite 5A will adsorb more of everything other than H_2 while adsorbing less H_2 when compared to CD-AC. However, the Zeolite 5A would still likely have to be used in combination with other sorbents to completely purify the H_2, since the Zeolite 5A does not adsorb CH_4 or CO strongly enough to remove all of them.

When analyzing the predicted loading values and comparing them with the experimentally observed multicomponent adsorption equilibrium data, the predicted values had varying levels of accuracy. In general, the predicted values were more accurate for the total adsorbed amounts than they were for the individual component adsorbed amounts, although there were multiple examples of exceptions to both of those takeaways. Of the materials looked at for the code validation section of the results, the

code was much better on average at predicting adsorbed amounts for activated carbon and MOFs than it was at predicting the adsorbed amounts for zeolites. This is likely the result of zeolites typically having more heterogeneous surfaces than activated carbons or MOFs, and the reasons for why surface heterogeneity can have such a large impact will be discussed shortly. The varying degrees of accuracy are likely caused by many factors. Among the contributing factors, some are significantly more likely to decrease the accuracy. Some of the factors with a heavier impact on the accuracy are the sorbent's characteristics, the polarity of the sorbate molecules in relation to one another, and the isotherm equation used to perform IAST calculations.

The specific sorbent characteristic that typically can impact predictions the most is whether the sorbent is heterogeneous or homogeneous since IAST uses the assumption that the surface of the sorbent is homogeneous. With a heterogeneous sorbent, different portions of the sorbent can adsorb differently from one another, meaning it is much more complicated to predict. Another factor that can impact the accuracy of the results is the relative polarities of the sorbate molecules. When using IAST, if one molecule is adsorbed much more strongly than others, it will likely "overpower" the other molecules in the resulting prediction. This is especially true of gases that are highly polar such as carbon dioxide. The last factor that will be discussed that can have a significant negative impact on the accuracy of the predicted loading is the isotherm equation used to perform IAST predictions and calculations. There are many different isotherm equations, and certain ones typically perform better under different conditions. Without having the experimental data, it is difficult to determine which isotherm equation should be used to perform multi-component adsorption equilibrium calculations. In this study, the isotherm

used for all calculations was the Langmuir isotherm equation. However, it is likely that in at least some of the calculations performed, a different isotherm equation would have been more accurate.

Recommendations for Future Work

There were several points during the process of writing the final code, generating data, and writing the thesis where things could likely be improved in future studies or efforts. First and foremost, finding proper data to use for the analysis of multicomponent adsorption equilibrium is extremely painful. Specifically, when looking for experimental data to compare predicted values with, it was very difficult to find papers or sources which provided not only enough pure gas adsorption equilibrium data to reconstruct those, but also enough mixed gas data to compare the generated predictions. Entire books have been written in the past which contain experimental adsorption equilibrium data for pure and mixed gases, but the ones that are easily accessible were written almost a quarter of a century ago (Valenzuela, 1989). A more modern online version of handbooks containing modern data like that would immensely speed up the process of generating mixed gas adsorption equilibrium data.

Another area that could be done better in the future is the actual methodology used for IAST calculations. Over the years, many researchers have scrutinized the original IAST method, and found certain ways of calculating things are slower than others. The project for this thesis focused on the classical IAST calculations, though there are certainly other calculation methods that could speed up processing time considerably (Landa et al., 2013). Similarly, the language used for this thesis, Python, is relatively

slow. Using a lower-level language such as C++ could speed up the processing time. With the quantity of data analysis performed in this thesis, processing time was not an issue, and as such, these two potentially more efficient methods were not utilized.

REFERENCES

Alazmi, A., Nicolae, S. A., Modugno, P., Hasanov, B. E., Titirici, M. M., & Costa, P. M. F. J. (2021). Activated Carbon from Palm Date Seeds for CO2 Capture. *International Journal of Environmental Research and Public Health*, *18*(22), 12142. https://doi.org/10.3390/ijerph182212142

Al-Naddaf, Q., Rownaghi, A. A., & Rezaei, F. (2020). Multicomponent adsorptive separation of CO2, CO, CH4, N2, and H2 over core-shell zeolite-5A@MOF-74 composite adsorbents. *Chemical Engineering Journal*, *384*, 123251. https://doi.org/10.1016/j.cej.2019.123251

A. Mason, J., Sumida, K., R. Herm, Z., Krishna, R., & R. Long, J. (2011). Evaluating metal–organic frameworks for post- combustion carbon dioxide capture via temperature swing adsorption. *Energy & Environmental Science*, *4*(8), 3030–3040. https://doi.org/10.1039/C1EE01720A

Avijegon, G., Xiao, G., Li, G., & May, E. F. (2018). Binary and ternary adsorption equilibria for CO2/CH4/N2 mixtures on Zeolite 13X beads from 273 to 333 K and pressures to 900 kPa. *Adsorption*, *24*(4), 381–392. https://doi.org/10.1007/s10450-018-9952-3

Ben-Mansour, R., Habib, M. A., Bamidele, O. E., Basha, M., Qasem, N. A. A., Peedikakkal, A., Laoui, T., & Ali, M. (2016). Carbon capture by physical adsorption: Materials, experimental investigations and numerical modeling and simulations – A review. *Applied Energy*, *161*, 225–255. https://doi.org/10.1016/j.apenergy.2015.10.011

Ben-Mansour, R., Qasem, N. A. A., & Antar, M. A. (2018). Carbon dioxide adsorption separation from dry and humid CO2/N2 mixture. *Computers & Chemical Engineering*, *117*, 221–235. https://doi.org/10.1016/j.compchemeng.2018.06.016

Carbon Storage FAQs. (n.d.). Netl.Doe.Gov. Retrieved April 3, 2022, from https://netl.doe.gov/coal/carbon-storage/faqs/carbon-storage-faqs

Carta, M. (2015). *Gas Separation* (pp. 852–855). https://doi.org/10.1007/978-3-642-40872-4_261-1

Cavenati, S., Grande, C. A., & Rodrigues, A. E. (2004). Adsorption Equilibrium of Methane, Carbon Dioxide, and Nitrogen on Zeolite 13X at High Pressures. *Journal of Chemical & Engineering Data*, *49*(4), 1095–1101. https://doi.org/10.1021/je0498917

Choi, S., Drese, J. H., & Jones, C. W. (2009). Adsorbent Materials for Carbon Dioxide Capture from Large Anthropogenic Point Sources. *ChemSusChem*, *2*(9), 796–854. https://doi.org/10.1002/cssc.200900036

Do, D. D. (1998). *Adsorption analysis: Equilibria and kinetics*. Imperial College Press.

Dubinin, M. M. (1960). The Potential Theory of Adsorption of Gases and Vapors for Adsorbents with Energetically Nonuniform Surfaces. *Chemical Reviews*, *60*(2), 235–241. https://doi.org/10.1021/cr60204a006

Flue gas properties table. (n.d.). Retrieved April 5, 2022, from https://www.pipeflowcalculations.com/tables/flue-gas.xhtml

Geankoplis, C. J. (2018). *Transport processes and separation process principles* (Fifth edition). Prentice Hall.

Hill, T. L. (1949). Statistical Mechanics of Adsorption. V. Thermodynamics and Heat of Adsorption. *The Journal of Chemical Physics*, *17*(6), 520–535. https://doi.org/10.1063/1.1747314

Hydrogen Production: Natural Gas Reforming. (n.d.). Energy.Gov. Retrieved April 6, 2022, from https://www.energy.gov/eere/fuelcells/hydrogen-production-natural-gas-reforming

Landa, H. O. R., Flockerzi, D., & Seidel-Morgenstern, A. (2013). A method for efficiently solving the IAST equations with an application to adsorber dynamics. *AIChE Journal*, *59*(4), 1263–1277. https://doi.org/10.1002/aic.13894

Marsh, H., & Rodríguez-Reinoso, F. (2006). *Activated carbon* (1st ed). Elsevier.

Myers, A. L., & Prausnitz, J. M. (1965). Thermodynamics of mixed-gas adsorption. *AIChE Journal*, *11*(1), 121–127. https://doi.org/10.1002/aic.690110125

Nieszporek, K. (2006). Application of the Vacancy Solution Theory to Describe the Enthalpic Effects Accompanying Mixed-Gas Adsorption. *Langmuir*, *22*(23), 9623–9631. https://doi.org/10.1021/la061847x

Pakseresht, S., Kazemeini, M., & Akbarnejad, M. M. (2002). Equilibrium isotherms for CO, CO2, CH4 and C2H4 on the 5A molecular sieve by a simple volumetric apparatus. *Separation and Purification Technology*, *28*(1), 53–60. https://doi.org/10.1016/S1383-5866(02)00012-6

Park, Y., Ju, Y., Park, D., & Lee, C.-H. (2016). Adsorption equilibria and kinetics of six pure gases on pelletized zeolite 13X up to 1.0MPa: CO2, CO, N2, CH4, Ar and H2. *Chemical Engineering Journal*, *292*, 348–365. https://doi.org/10.1016/j.cej.2016.02.046

Park, Y., Moon, D.-K., Kim, Y.-H., Ahn, H., & Lee, C.-H. (2014). Adsorption isotherms of CO2, CO, N2, CH4, Ar and H2 on activated carbon and zeolite LiX up to 1.0 MPa. *Adsorption*, *20*(4), 631–647. https://doi.org/10.1007/s10450-014-9608-x

Principe, I. A., & Fletcher, A. J. (2020). Adsorption selectivity of CO2 over CH4, N2 and H2 in melamine–resorcinol–formaldehyde xerogels. *Adsorption*, *26*(5), 723–735. https://doi.org/10.1007/s10450-020-00203-w

Ray, M. S. (1996). Diffusion in Zeolites and Other Microporous Solids, by J. Karger and D. M. Ruthven, John Wiley, New York, USA (1992). 605 pages. ISBN 0-47 1-50907-8. *Developments in Chemical Engineering and Mineral Processing*, *4*(3–4), 254–254. https://doi.org/10.1002/apj.5500040311

Reich, R., Ziegler, W. T., & Rogers, K. A. (1980). Adsorption of Methane, Ethane, and Ethylene Gases and Their Binary and Ternary Mixtures and Carbon Dioxide on Activated Carbon at 212-301 K and Pressures to 35 Atmospheres. *Industrial & Engineering Chemistry Process Design and Development*, *19*(3), 336–344. https://doi.org/10.1021/i260075a002

Rother, J., & Fieback, T. (2013). Multicomponent adsorption measurements on activated carbon, zeolite molecular sieve and metal–organic framework. *Adsorption*, *19*(5), 1065–1074. https://doi.org/10.1007/s10450-013-9527-2

Sabouni, R., Kazemian, H., & Rohani, S. (2013). Carbon dioxide adsorption in microwave-synthesized metal organic framework CPM-5: Equilibrium and kinetics study. *Microporous and Mesoporous Materials*, *175*, 85–91. https://doi.org/10.1016/j.micromeso.2013.03.024

Simon, C. M., Smit, B., & Haranczyk, M. (2016). pyIAST: Ideal adsorbed solution theory (IAST) Python package. *Computer Physics Communications*, *200*, 364–380. https://doi.org/10.1016/j.cpc.2015.11.016

Sircar, S. (1999). Gibbsian Surface Excess for Gas AdsorptionRevisited. *Industrial & Engineering Chemistry Research*, *38*(10), 3670–3682. https://doi.org/10.1021/ie9900871

Sircar, S. (2006). Basic Research Needs for Design of Adsorptive Gas Separation Processes. *Industrial & Engineering Chemistry Research*, *45*(16), 5435–5448. https://doi.org/10.1021/ie051056a

Talu, O., & Zwiebel, I. (1986). Multicomponent adsorption equilibria of nonideal mixtures. *AIChE Journal*, *32*(8), 1263–1276. https://doi.org/10.1002/aic.690320805

Thiele, H. (1953). The Dynamical Character of Adsorption, von H. J. de Boer. Oxford University Press, 1953. 1. Aufl. X V, 239 S., 45 Abb. Gebd. S. 30.—. *Angewandte Chemie*, *65*(16), 431–431. https://doi.org/10.1002/ange.19530651619

US EPA, O. (2016, January 12). *Global Greenhouse Gas Emissions Data* [Overviews and Factsheets]. https://www.epa.gov/ghgemissions/global-greenhouse-gas-emissions-data

Valenzuela, D. P. (1989). *Adsorption equilibrium data handbook / Diego P. Valenzuela, Alan L. Myers.* Prentice Hall.

Wang, Y., & LeVan, M. D. (2010). Adsorption Equilibrium of Binary Mixtures of Carbon Dioxide and Water Vapor on Zeolites 5A and 13X. *Journal of Chemical & Engineering Data*, *55*(9), 3189–3195. https://doi.org/10.1021/je100053g

Watson, G. C., Jensen, N. K., Rufford, T. E., Chan, K. I., & May, E. F. (2012). Volumetric Adsorption Measurements of N2, CO2, CH4, and a CO2 + CH4 Mixture on a Natural Chabazite from (5 to 3000) kPa. *Journal of Chemical & Engineering Data*, *57*(1), 93–101. https://doi.org/10.1021/je200812y

Yang, R. T. (2003). *Adsorbents: Fundamentals and Applications*. John Wiley & Sons, Inc. https://doi.org/10.1002/047144409X

Zhang, Y., Su, W., Sun, Y., Liu, J., Liu, X., & Wang, X. (2015). Adsorption Equilibrium of N2, CH4, and CO2 on MIL-101. *Journal of Chemical & Engineering Data*, *60*(10), 2951–2957. https://doi.org/10.1021/acs.jced.5b00327

APPENDIX A

PYTHON FILE USED FOR DATA SELECTION

```
# This file creates multiple GUIs to allow for data selection and
parameter specification for multicomponent adsorption
# Created by: Trevor Ciha

import PySimpleGUI as sg
import pandas as pd

# Setting GUI color scheme
sg.theme('Dark Grey 13')

# Field names for GUI inputs of first window
FN_COMPONENTS = 'Number of Components Adsorbing'
FN_MAX_PRESSURE = 'Max Output Pressure'
FN_MIN_PRESSURE = 'Min Output Pressure'
FN_PRESSURE_INT = 'Output Pressure Intervals'
FN_PRESSURE_UNITS = 'Units of Pressure from Isotherms'
FN_LOADING_UNITS = 'Units of Loading from Isotherms'

# Putting field names in a list to allow for indexing them easily
FIELD_NAMES =
[FN_COMPONENTS,FN_MAX_PRESSURE,FN_MIN_PRESSURE,FN_PRESSURE_INT,FN_PRESSURE
_UNITS,FN_LOADING_UNITS]

# Defining number of fields for indexing
NUM_FIELDS = 6

layout = []
# For loop that creates input text boxes for first window
for index in range(NUM_FIELDS):
    layout.append([sg.Text(FIELD_NAMES[index]+': ',size=(25,1)),
sg.InputText(key=FIELD_NAMES[index],size=(10,1))])
layout.append([sg.OK(), sg.Cancel()])

# Creating, opening, and closing the first GUI window
window = sg.Window('Get Parameters', layout)
event, values = window.read()
window.close()

# Taking user inputs from GUI and renaming them for ease of use along with
changing data types for math usage
number_components = int(values[FN_COMPONENTS])
max_pressure = float(values[FN_MAX_PRESSURE])
min_pressure = float(values[FN_MIN_PRESSURE])
pressure_interval = float(values[FN_PRESSURE_INT])
```

```
pressure_units = values[FN_PRESSURE_UNITS]
loading_units = values[FN_LOADING_UNITS]


layout = []
# For loop that creates the input boxes and labels for second window
for index in range(number_components):
    layout.append([sg.Text(f'Filename for Data of Component {index+1}:')])
    layout.append([sg.Input(key=f'data{index}'), sg.FileBrowse()])
    layout.append([sg.Text(f'Gas Mol Fraction for Component {index+1}:'),
sg.InputText(key=f'frac{index}',size=(14,1))])
    layout.append([sg.Text(f'Name of Component {index+1}:'),
sg.InputText(key=f'name{index}',size=(14,1))])
    layout.append([sg.Text()])
layout.append([sg.OK(), sg.Cancel()])

# Creating, opening, and closing the second GUI window
window = sg.Window('Get Adsorption Data', layout)
event, values = window.read()
window.close()

raw_data = []
gas_mol_fractions = []
gas_names = []
# For loop that takes all user inputs from second window and organizes &
renames them for later use
for index in range(number_components):
    raw_data.append(pd.read_csv(values[f'data{index}']))
    gas_mol_fractions.append(float(values[f'frac{index}']))
    gas_names.append(values[f'name{index}'])
```

APPENDIX B

PYTHON FILE USED FOR ISOTHERM CONSTANTS

```
# This file takes user-inputted data from csv files and fits the desired
isotherm model to it
# Created by: Trevor Ciha

from scipy.optimize import curve_fit
from Data_Selection import *
import pandas as pd
import numpy as np
from sys import exit

raw_data = []
# For loop that takes all user inputs from second window and organizes &
renames them for later use
for index in range(number_components):
     raw_data.append(pd.read_csv(gas_data_files[index]))

# Langmuir isotherm equation used for fitting
def langmuir_fit_func(x,a,b):
    return (a*b*x)/(1+b*x)

parameters = []
# For loop that fits each component's isotherm data to the desired
isotherm model
for component in raw_data:
    total_array = component.to_numpy()
    pressure_array = total_array[:,0]
    loading_array = total_array[:,1]
    popt, pcov =
curve_fit(langmuir_fit_func,pressure_array,loading_array,[100,1],bounds=(0
.0001,np.inf))
    parameters.append(popt)

gas_parameters = []
# For loop that organizes isotherm parameters and mol fractions of each
component for easier use later
for index, value in enumerate(parameters):
    gas_temp = []
    gas_temp.append(value[0])
    gas_temp.append(value[1])
    gas_temp.append(gas_mol_fractions[index])
    gas_parameters.append(gas_temp)
```

APPENDIX C

PYTHON FILE USED FOR IAST CALCULATIONS

```
# This file takes isotherm constants and calculates adsorbed
concentrations
# Created by: Trevor Ciha

import numpy as np
from scipy.integrate import quad
import matplotlib.pyplot as plt
from Isotherms import *

# Defining max iterations and tolerance for Newton-Raphson method
max_iter = 100000
tol = 0.000001

# Function for integrating Langmuir equation to obtain initial guess of
spreading pressure
def guess_integrator(x,indiv_gas,gas_parameters):
    denominator = 0
    for gas in gas_parameters:
        denominator += (gas[1]*gas[2])
    y = (indiv_gas[0]*(indiv_gas[1]*indiv_gas[2]*x)/(1+x*denominator))/x
    return y

# Langmuir Isotherm Equation for calculating amount adsorbed
def langmuir(gas,gas_pressure):
    y = (gas[0]*(gas[1]*gas_pressure)/(1+gas[1]*gas_pressure))
    return y

# Function used to calculate numerator of Newton-Raphson method, F(z_k)
def z_k_function(gases,pressures):
    component_sum = 0
    for index, gas in enumerate(gases):
        indiv_component = (total_pressure*gas[2])/(pressures[index])
        component_sum += indiv_component
    F_z_k = component_sum - 1
    return F_z_k

# Function used to calculate denominator of Newton-Raphson method, F'(z_k)
def z_k_prime_function(gases,pressures):
    component_sum = 0
    for index, gas in enumerate(gases):
        indiv_component =
(total_pressure*gas[2])/(pressures[index]*langmuir(gas,pressures[index]))
        component_sum += indiv_component
    F_z_k_prime = -component_sum
```

```
    return F_z_k_prime

# Function used to calculate the pure pressure of a component using the
spreading pressure
def pure_pressure_function(z_val,gas):
    pure_pressure = (1/gas[1])*(np.exp(z_val/gas[0])-1)
    return pure_pressure

# Creating the plot labels and titles
plt.subplot(2,1,1)
plt.xlabel(f'Pressure ({pressure_units})')
plt.ylabel(f'Loading ({loading_units})')
plt.title('Multicomponent Adsorption Isotherms')

# Generating pressure range to calculate adsorbed quantity for
pressure_range = np.arange(min_pressure,max_pressure,pressure_interval)

total_loading = []
all_adsorbed_amounts = []
# For loop to generate adsorbed concentrations across range of pressures
for total_pressure in pressure_range:

    z = 0
    # Iterating through the gases to calculate the initial guess for
spreading pressure (z)
    for gas in gas_parameters:
        z_temp, err =
quad(guess_integrator,0,total_pressure,args=(gas,gas_parameters))
        z += gas[2]*z_temp

    tolerance = True
    iter = 0
    # While loop used to perform Newton-Raphson method to calculate
spreading pressure
    while tolerance:
        iter += 1
        pure_pressures = []

        # Calculating pure pressure of each component from spreading
pressure
        for gas in gas_parameters:
            pure_pressures.append(pure_pressure_function(z,gas))

        # Calculating new spreading pressure with Newton-Raphson method
```

```
        new_z_val = z -
z_k_function(gas_parameters,pure_pressures)/z_k_prime_function(gas_paramet
ers,pure_pressures)

        # Checking if either stopping condition has been met
        if (abs(z - new_z_val) < tol) or (iter > max_iter):
            tolerance = False

        z = new_z_val

    adsorbed_mol_fractions = []
    # Calculating adsorbed mol fractions using Raoult's Law
    for index, gas in enumerate(gas_parameters):
        x = (total_pressure*gas[2]/pure_pressures[index])
        adsorbed_mol_fractions.append(x)

    inv_total_adsorbed = 0
    # Calculating the inverse of the total quantity adsorbed using the
isotherm model
    for index, gas in enumerate(gas_parameters):
        adsorbed_term =
adsorbed_mol_fractions[index]/langmuir(gas,pure_pressures[index])
        inv_total_adsorbed += adsorbed_term

    # Calculating total adsorbed quantity
    total_adsorbed = inv_total_adsorbed**-1

    total_loading.append(total_adsorbed)


    component_adsorbed = []
    # Calculating quantity adsorbed of each component
    for index in range(len(gas_parameters)):
        component_adsorbed.append(adsorbed_mol_fractions[index]*total_adso
rbed)

    # Putting list of adsorbed quantities for each component at the
current pressure into a list
    all_adsorbed_amounts.append(component_adsorbed)

# For loop that plots data series for each component
for index, gas in enumerate(gas_names):
    adsorbed_series = []
    for value in all_adsorbed_amounts:
```

```
            adsorbed_series.append(value[index])
        plt.plot(pressure_range,adsorbed_series,label=f'{gas_names[index]}')
    plt.plot(pressure_range,total_loading,label='Total Loading',ls='--')
    plt.legend()

    selectivity = []
    for value in all_adsorbed_amounts:
        selectivity.append(value[0]/value[1])

    with open('results.csv','w') as f:
        f.write(f'Pressure ({pressure_units})')
    for index in range(number_components):
        with open('results.csv','a') as f:
            f.write(f',{gas_names[index]} Loading ({loading_units})')
    with open('results.csv','a') as f:
        f.write('\n')

    for index in range(len(pressure_range)):
        with open('results.csv','a') as f:
            f.write(f'{pressure_range[index]}')
        for idx in range(number_components):
            with open('results.csv','a') as f:
                f.write(f',{all_adsorbed_amounts[index][idx]}')
        with open('results.csv','a') as f:
            f.write('\n')

    plt.subplot(2,1,2)
    plt.plot(pressure_range,selectivity,label='CO2/N2 selectivity')
    plt.xlabel(f'Pressure ({pressure_units})')
    plt.ylabel(f'CO2/N2 Selectivity')
    plt.title('Selectivity')
    plt.show()
```